

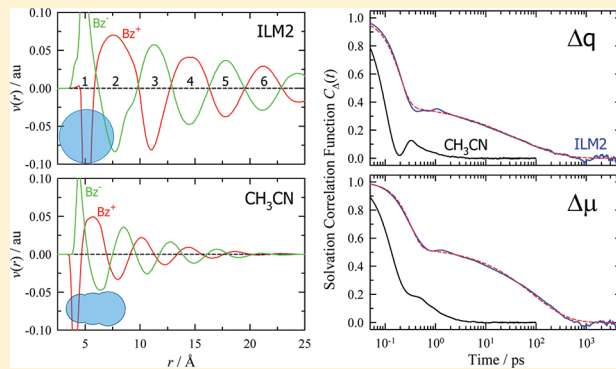
Simulations of Solvation and Solvation Dynamics in an Idealized Ionic Liquid Model

Durba Roy[†] and Mark Maroncelli*

Department of Chemistry, The Pennsylvania State University, University Park, Pennsylvania 16802, United States

Supporting Information

ABSTRACT: Equilibrium and nonequilibrium molecular dynamics simulations of solvation and solvation dynamics of a variety of solutes have been performed in the coarse-grained ionic liquid model ILM2 (Roy, D.; Maroncelli, M. *J. Phys. Chem. B* **2010**, *114*, 12629). Some comparisons are made between ionic and dipolar solvation using parallel simulations in CH₃CN. Despite the fact that the multipolar character of electrostatic interactions and their spatial extent differ in the two solvents, solvation energies are equal to within about 10% in ILM2 and CH₃CN. This near equality also holds with reduced accuracy in the case of reorganization energies. Solvation energies of spherical solutes in ILM2 and its variants can be correlated as a function of solute and solvent size using a Born-type expression with an effective cavity size. Solvation time correlation functions in ILM2 exhibit a subpicosecond inertial component followed by a broadly distributed component related to solvent viscosity, comparable to what has been observed in experiment. Direct comparison of simulation to experiment using the solute coumarin 153 (C153) shows general agreement on the time scales and character of the fast and slow components, but the amplitude of the fast component is overestimated by the simulations. Solute motion can significantly increase the speed of solvation, even in the case of large solutes such as C153. Good agreement is found between linear response estimates and the nonequilibrium dynamics associated with electronic excitation of C153. In contrast, perturbations involving changes of a full electron charge in atomic solutes lead to local heating which greatly hastens solvation compared to linear response predictions. The mechanism of charge solvation in atomic solutes is examined in some detail. It is found that ion translation dominates the inertial dynamics. The rotational contribution only becomes comparable to the translation contribution in the tail of the response. Adjustments of ion positions over distances of ~30% of their diameters are all that is required to relax the solvation energy in these systems.



1. INTRODUCTION

Ionic liquids are finding increasing use as solvents for chemical and biochemical reactions,^{1,2} in analytical separations,³ and in a variety of electrochemical⁴ and energy-related contexts.⁵ Motivated by these latter applications, a number of groups have sought to probe the nature of electrostatic solvation in ionic liquids^{1,6–13} and learn how the purely ionic environment presented by these solvents affects charge-transfer processes.^{14–18} The picture emerging from these studies is that whereas the solvation energies of polar molecules and ions in ionic liquids are comparable to those found in high-polarity conventional solvents like acetonitrile or methanol,^{1,6,19} the dynamics of solvation are distinctive. In contrast to most conventional solvents, where equilibrium solvation energies are established within a few picoseconds after an electrostatic perturbation, solvent equilibration extends to nanosecond times in ionic liquids. In addition, solvation energy relaxation is a broadly distributed process involving important contributions on time scales ranging from 100 fs to 10 ns or more.^{6,8,9,20,17,21} This slow and broadly distributed solvent response results in charge-transfer and other fast processes exhibiting heteroge-

neous dynamics unlike what is found in conventional room-temperature solvents.^{22–24,17,25} Understanding this response is therefore an important prerequisite to modeling fast reactions in this new class of solvent.

The present paper reports computer simulations designed to provide a better understanding of the molecular features that give rise to the distinctive solvation response of ionic liquids. A large body of published literature already exists on the use of computer simulations to study ionic liquids. Such simulations have been performed for over a decade now,^{26,27} and a number of recent studies have focused on some of the aspects of electrostatic solvation of interest here.^{28–52} Lynden-Bell⁴⁷ compared the energetics of charging a small atomic solute over the range from $-3e$ to $+3e$ in acetonitrile and two ionic liquids, 1,3-dimethylimidazolium chloride and hexafluorophosphate, in order to investigate the applicability of Marcus theory in purely ionic media. (For brevity, we hereafter use the

Received: February 10, 2012

Revised: April 13, 2012

Published: April 19, 2012

notation Im_{mn}^+ to denote a 1,3-dialkylimidazolium cation with n -alkyl groups of m and n carbon atoms. Using this notation the aforementioned ionic liquids are denoted $[\text{Im}_{11}][\text{Cl}]$ and $[\text{Im}_{11}][\text{PF}_6]$.) Consistent with Marcus theory, Lynden-Bell observed nearly parabolic free energy profiles and reorganization and activation energies for one-electron processes close to expectations of Marcus theory. She also noted that these energies and their dependence on solute charge was nearly the same in these ionic liquids and in acetonitrile, underscoring the energetic similarity between ionic liquids and high-polarity conventional solvents found experimentally. In another study⁴⁹ Lynden-Bell examined how solvation energies depend upon solute size and shape and emphasized the effectiveness of charge screening in ionic liquid solvents. Lynden-Bell and co-workers also reported preliminary simulations of the short-time dynamics of solvation of atomic solutes⁵⁰ and the related phenomenon of polarization relaxation of a model ionic liquid capacitor.⁴⁸

In an extensive series of papers, Shim, Kim, and co-workers reported simulations of a model diatomic molecule undergoing transitions between a nondipolar (NP) state and a highly dipolar ion-pair (IP) state in $[\text{Im}_{21}][\text{Cl}]$ and $[\text{Im}_{21}][\text{PF}_6]$.^{28–35} In seminal work they probed the solvation structures and energies^{28,29} of the NP and IP solutes as well as the equilibrium and nonequilibrium solvation dynamics related to $\text{NP} \leftrightarrow \text{IP}$ transitions.³⁰ These simulations were the first to show that charge transfer in ionic liquids leads to a highly biphasic response in which more than one-half of the solvation energy relaxes via a subpicosecond inertial component followed by a much slower response due to diffusive ion motions. The presence of a significant subpicosecond component was subsequently confirmed in experiment⁵³ but with a much smaller amplitude than indicated by simulation. Shim et al.³⁰ also investigated the mechanisms of solvation and showed that, especially in $[\text{Im}_{21}][\text{Cl}]$, the rapid response is dominated by translational motions of the Cl^- anions. Further work by this same group extended simulations to longer times,⁵⁴ made comparisons to dielectric continuum predictions,³⁴ and investigated the effects of solute polarizability³¹ on the solvation response in $[\text{Im}_{21}][\text{PF}_6]$. They also investigated the energetics³² and kinetics³³ of the $\text{NP} \leftrightarrow \text{IP}$ charge-transfer process in the context of Marcus and Grote–Hynes⁵⁵ theories. Additional studies of NP and IP rotational diffusion⁵⁶ and vibrational relaxation⁵⁷ in $[\text{Im}_{21}][\text{PF}_6]$ provide for a wonderfully complete description of one example of a model solute/ionic liquid system.

Other researchers simulated several solutes used in experimental studies of solvation and charge transfer.^{42–45,36–40,52} Margulis and co-workers focused mainly on simulations of heterogeneity in ionic liquids. Their work^{42,43} showed how the distribution of solvation energies in long-lived local environments in liquid $[\text{Im}_{41}][\text{PF}_6]$ at room temperature lead to excitation dependence of the emission of the solvatochromic probe 2-amino-7-nitrofluorenone.⁵⁸ Their later work provided a demonstration of the way in which such energetic heterogeneity can lead to rate heterogeneity in fast electron transfer reactions.⁴⁵

In early studies, Kobrak and Znamenskiy^{36,37} simulated spectral shifts of the popular polarity probe betaine-30 in $[\text{Im}_{41}][\text{PF}_6]$ and stressed the collective nature of the solvation response in ionic liquids. Kobrak later simulated the fluorescence probe coumarin 153 (C153),^{38–40} which has long been the probe of choice for measuring the dynamics of

nonspecific polar solvation.⁵⁹ One interesting aspect of this work was observation of a much more modest (12–24%) subpicosecond component to the solvation response of this polyatomic solute compared to the >50% responses reported for atomic⁵⁰ and diatomic^{30,46} solutes. These smaller amplitude inertial components are closer to what has been observed experimentally for polyatomic solutes.^{9,17,8} Kobrak also performed a detailed analysis of the short-time behavior of equilibrium solvation time correlation functions (tcfs) of C153 in $[\text{Im}_{41}][\text{PF}_6]$ ^{38,39} and two N,N -dialkyl pyrrolidinium ionic liquids $[\text{Pr}_{41}][\text{Br}]$ and $[\text{Pr}_{41}][\text{Tf}_2\text{N}]$.⁴⁰ (Tf_2N^- denotes the bis(trifluoromethanesulfonyl)imide anion.) Their analysis showed that even the initial ultrafast response involved significant contributions from anticorrelated cation–anion motions. At least on the fast time scales accessible to their analysis, rotational motion was found to play a minor role in solvation.

In the present work we employ a coarse-grained model of an ionic liquid, “ILM2”,^{60,61} to further explore basic aspects of solvation in ionic liquids. ILM2 consists of a three-site cation and single-site anion roughly corresponding to Im_{41}^+ and PF_6^- . Despite its simplicity, this model has been shown to possess temperature-dependent volumetric, transport,⁶¹ and interfacial⁶² properties in good agreement with those measured for the prototypical ionic liquid $[\text{Im}_{41}][\text{PF}_6]$. Although we make some comparisons to experimental solvation data in $[\text{Im}_{41}][\text{PF}_6]$, we use ILM2 here primarily as a low-cost generic model expected to display most of characteristic features of solvation in real ionic liquids. The simplicity of this model enables study of a variety of solutes and conditions over the nanosecond time scales comparable to those used in experiments. As has been done in several past studies,^{47,49,32,54,33} we also perform parallel simulations in the prototypical dipolar solvent CH_3CN ⁶³ in order to highlight some of the similarities and differences between solvation in ionic versus dipolar media.

After describing the simulation potentials and methods in section 2, the results of this work are discussed in four parts. Section 3.A involves structural aspects of solvation, in particular, the similarities and differences in the charge ordering present in ILM2 and CH_3CN . Section 3.B concerns electrostatic solvation energies. Despite the different multipole character and thus range of electrostatic interactions, these simulations show the solvation energies of a variety of solutes to be remarkably similar in the two solvents. The results of this section also provide some guidance for predicting how electrostatic energies depend on solute size. In section 3.C we consider the time-dependent fluctuations in electrostatic quantities that form the linear response estimates of the solvation response to various electrostatic perturbations. Whereas both solvents exhibit strongly biphasic dynamics, consisting of a prominent subpicosecond inertial component and a slower diffusive component, like experiment, we find the time scales of the diffusive component to be orders of magnitude slower in ILM2 compared to CH_3CN . The computational economy of ILM2 enables us to explore the dependence of both the inertial and the diffusive components on solute size, perturbation type, and temperature. We also make the first direct comparisons between experiment and simulations using recent experimental data on the solute C153,⁸ consider how solute motion influences solvation, and test the applicability of linear response approaches for predicting the solvation dynamics. Finally, in section 3.D we discuss in some detail the mechanisms underlying the solvation response in

ionic liquids for the simplest case of charge solvation in an atomic solute.

2. SIMULATION POTENTIALS AND METHODS

All molecules simulated here consist of rigid bodies interacting through site–site potentials of the standard Lennard–Jones (6–12) plus Coulomb form, with Lorentz–Berthelot combining rules used to determine interaction parameters of unlike pairs. The potential parameters of the ionic liquid ILM2 are described in ref 61 and those of acetonitrile in ref 63. Figure 1

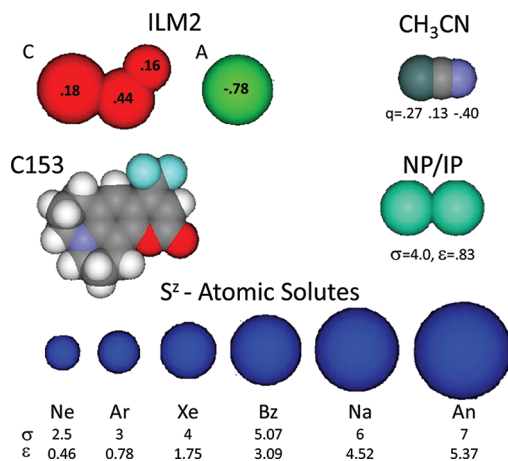


Figure 1. Schematic of the solvent and solute models studied. van der Waals surfaces of all molecules are shown to the same scale. Atomic charges of the solvents ILM2 and CH_3CN are shown as are the Lennard–Jones parameters of the atomic solutes (with σ in Å and ϵ in kJ/mol).

shows space-filling representations of these solvents together with the solutes examined. Most simulations described here involve the series of single-site solutes denoted S^z (with $z = 0, \pm 1e$). As indicated by the labels “Ne”, “Ar”, and “Xe”, the smaller members of this series have Lennard–Jones parameters appropriate to rare gas atoms. The larger members, “Bz”, “Na”, and “An”, were constructed to have volumes and energy parameters roughly appropriate to benzene, naphthalene, and anthracene. These solutes were held immobile during simulations in order to eliminate the effects of solute motions on the observed dynamics. We also briefly examined the solutes coumarin 153 (C153) and the diatomic “NP/IP” solute studied in detail by Shim and Kim.^{28–30,56,57,32,54,34,33} A complete listing of potential parameters for C153 can be found in ref 64. The charge distributions used to represent the S_0 and S_1 electronic states of this solute provide dipole moments of 6.2 and 13.6 D, respectively. The NP/IP solutes consist of Lennard–Jones interaction sites separated by 3.5 Å with no charges (NP) or full $\pm e$ charges (IP) which produces a dipole moment of 16.8 D.

To explore the effect of solvent size on solvation energies, we also performed a limited number of simulations using scaled versions of ILM2. Solvent models were created by scaling bond lengths (\tilde{l}_{ij}), Lennard–Jones parameters (σ_i, ϵ_i), and masses (m_i) of the original model in the manner $\tilde{l}_{ij} = \lambda l_{ij}$, $\tilde{\sigma}_i = \lambda \sigma_i$, $\tilde{\epsilon}_i = \lambda^3 \epsilon_i$, and $\tilde{m}_i = \lambda^3 m_i$ with scale factors $\lambda = 0.75, 1.25$, and 1.5 . This scaling creates a set of liquids having masses and Lennard–Jones energy densities comparable to ILM2 but with scaled charge densities. The range of λ values was chosen to span a range of sizes characteristic of ionic liquids from

ethylammonium nitrate ($\lambda \approx 0.7$) to trihexyltetradecylphosphonium bis(trifluoromethylsulfonyl)imide ($\lambda \approx 1.5$).

Molecular dynamics simulations were performed using a modified version of the DL POLY_2 code.⁶⁵ Cubic periodic boundary conditions were used on systems consisting of one solute and either 343 ILM2 ion pairs or 512 CH_3CN molecules. Time steps of 5 and 2 fs were used for ILM2 and CH_3CN , respectively. Equilibrium simulations were performed in NPT ensembles at 1 bar pressure and temperatures between 300 and 550 K. Most results reported here were collected at 350 K, and this temperature should be assumed unless stated otherwise. The Nose–Hoover (Melchionna) algorithms with relaxation times of 0.5 and 2.0 ps were used for the thermostat and barostat, respectively. All nonbonded interactions were calculated within a spherical distance cutoff of 16.0 Å using a Verlet neighbor list with a shell width of 2.0 Å. The standard Ewald method with automatic parameter optimization was used to calculate electrostatic interactions for the MD simulations. In order to effect separation of cation and anion contributions to the solvation energy, solute–solvent electrostatic interactions were also calculated using an eighth-order Kubic harmonic approximation to the Ewald summation.⁶⁶ In the case of charged solutes both methods adopt a uniform background of neutralizing charge to remove the divergence of the lattice sum.

The starting configurations for the equilibrium simulations were obtained from an expanded lattice of ion pairs with the solute embedded within it. The system was equilibrated first at high temperature (450 K) followed by reduction to the temperature of interest (300–425 K) where further equilibration for at least 100 ns was performed prior to data collection. Data were collected for a period of 250 ns in 5 ns blocks. Block averages were used to estimate statistical uncertainties in the data, which are reported as 2 times the standard deviation of the mean.

The nonequilibrium simulations of solvation dynamics described below were performed in the NVE ensemble beginning from 500 initial conditions sampled from equilibrium simulations of the initial solute state. For these simulations a step size of 1 fs and run length of 1 ns (ILM2) or 100 ps (CH_3CN) were used.

Both equilibrium and nonequilibrium simulations of solvation dynamics were performed. The nonequilibrium simulations directly model the sort of process studied in dynamic Stokes shift experiments. For these simulations a set of quasi-independent starting points was collected from an equilibrium ensemble with the solute in an initial charge state “0”. At time zero the solute state was switched to state “1” and each starting point then propagated for an appropriate length of time. The observable of interest is the difference in the electrostatic solute–solvent interaction energy as a function of time, $\Delta U_{\text{EI}}(t) = U_1^{\text{EI}}(t) - U_0^{\text{EI}}(t)$. This difference averaged ($\langle \rangle$) over the ensemble of nonequilibrium trajectories provides the magnitude of the solvation response⁶⁷

$$\langle \Delta U_{\text{EI}}(0) - \Delta U_{\text{EI}}(\infty) \rangle_{0 \rightarrow 1}^{\text{ne}} \cong \langle \Delta U_{\text{EI}} \rangle_0^{\text{eq}} - \langle \Delta U_{\text{EI}} \rangle_1^{\text{eq}} \quad (1)$$

The time dependence of solvation is characterized by the solvation response function

$$S_{\Delta}(t) = \frac{\langle \Delta U_{\text{EI}}(t) - \Delta U_{\text{EI}}(\infty) \rangle_{0 \rightarrow 1}^{\text{ne}}}{\langle \Delta U_{\text{EI}}(0) - \Delta U_{\text{EI}}(\infty) \rangle_{0 \rightarrow 1}^{\text{ne}}} \quad (2)$$

This dynamics can also be approximated using only information from equilibrium simulations under the assumption that the solvent response is linear or Gaussian. The relations are^{68–70}

$$\langle \Delta U_{\text{El}}(t) - \Delta U_{\text{El}}(\infty) \rangle_{0 \rightarrow 1}^{\text{ne}} \cong \frac{\langle \delta \Delta U_{\text{El}}(0) \delta \Delta U_{\text{El}}(t) \rangle_{0 \text{ or } 1}^{\text{eq}}}{k_B T} \quad (3)$$

where $\delta \Delta U_{\text{El}}(t) \equiv \Delta U_{\text{El}}(t) - \langle U_{\text{El}} \rangle_i^{\text{eq}}$ and $\langle \cdot \rangle_i^{\text{ne}}$ and $\langle \cdot \rangle_i^{\text{eq}}$, respectively, denote nonequilibrium and equilibrium averages over an ensemble in the presence of solute state $i = 0$ or 1 . The linear response equivalent of $S_{\Delta}(t)$ is the solvation time correlation function

$$C_{\Delta}^{(i)}(t) \equiv \frac{\langle \delta \Delta U_{\text{El}}(0) \delta \Delta U_{\text{El}}(t) \rangle_i}{\langle (\delta \Delta U_{\text{El}})^2 \rangle_i} \quad (4)$$

Approximating the nonequilibrium response using the equilibrium dynamics of the initial state (subscript 0 on the right side of eq 3) results from standard application of linear response theory,⁶⁸ whereas use of the final state can be justified either by a simple modification of the linear response formalism⁶⁹ or by invoking the more general assumption that $\delta \Delta U_{\text{El}}(t)$ is Gaussian.⁷⁰

In the case of charged solutes, there is a significant dependence of the electrostatic solvation energy on system size. Several groups have examined this effect in simulations using periodic boundary conditions and the Ewald approach to treating long-range interactions.^{71–74} It has been shown that infinite system energies can be estimated with good accuracy using the relation^{72,75}

$$\langle U_{\text{El}} \rangle_{\infty} \cong \langle U_{\text{El}} \rangle_L - q^2 \left(1 - \frac{1}{\epsilon_r} \right) \left(\frac{\xi}{L} - \frac{2\pi R^2}{3L^3} \right) \quad (5)$$

where L denotes the periodic cell length, $\xi = 2.837$ for a cubic cell, ϵ_r is the relative permittivity of the solvent, and q and R denote the solute charge and radius. We examined the size dependence of simulated electrostatic energies over a limited range of sizes ($N = 170$ – 500 ion pairs; $L = 39$ – 56 Å), and it appears that eq 5 applies to ionic solvents as well as to the dipolar solvents previously examined. In the cases studied here the R dependence in eq 5 is negligible and the appropriate value of $\epsilon_r = \infty$, so that the simplified version

$$\langle U_{\text{El}} \rangle_{\infty} \cong \langle U_{\text{El}} \rangle_L - q^2 \frac{\xi}{L} \quad (6)$$

applies. For the systems of 343 ion pairs ($L = 50$ Å) studied here the correction amounts to -79.3 kJ/mol, which is 15–30% of the solvation energies of the charged atomic solutes S^+ and S^- . The system size will also affect fluctuations in the energy of a charged solute, and to correct for this effect we follow the practice of Hummer et al.⁷¹ and assume that the correction for $\langle \delta U_{\text{El}}^2 \rangle$ and $\langle U_{\text{El}} \rangle$ are related by linear response

$$\langle \delta U_{\text{El}}^2 \rangle_{\infty} \cong \langle \delta U_{\text{El}}^2 \rangle_L + q^2 k_B T \frac{\xi}{L} \quad (7)$$

In what follows, electrostatic ion solvation energies and their fluctuations are provided after application of these corrections.

3. RESULTS AND DISCUSSION

3.A. Solvation Structure. Figure 2 and Table 1 provide an overview of the structural features observed in the solvation of positively charged atomic solutes S^+ in ILM2 at 350 K. Figure 2

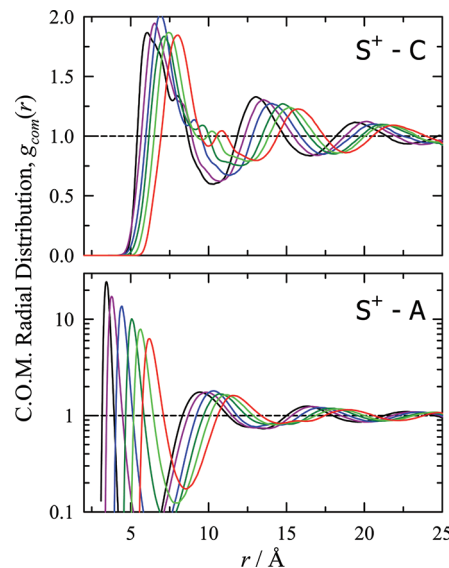


Figure 2. Center-of-mass radial distribution functions between positively charged solutes S^+ and cations (C, top) and anions (A, bottom) of ILM2 at 350 K. Solute size increases from left to right: Ne^+ , Ar^+ , Xe^+ , Bz^+ , Na^+ , and An^+ .

Table 1. Characteristics of the Solvation Structure of S^+ Solutes

A. characteristics of $g_{\text{com}}(r)$ functions ^a							
solute	$r_{\text{max}}/\text{\AA}$	$R_1/\text{\AA}$	$N_A(R_1)$	$N_C(R_1)$	$R_2/\text{\AA}$	$N_A(R_2)$	$N_C(R_2)$
Ne^+	3.4	5.1	4.1	0.0	10.3	15	12
Ar^+	3.8	6.0	4.6	0.8	10.8	17	14
Xe^+	4.4	6.6	5.6	1.7	11.4	20	16
Bz^+	5.1	7.3	6.4	3.5	12.1	23	20
Na^+	5.7	7.9	7.2	4.9	12.4	25	21
An^+	6.3	8.5	8.2	6.2	13.0	28	24

B. distributions of the first-shell anion coordination numbers ^b									
N _A									
	3	4	5	6	7	8	9	10	
Ne^+	0.08	99.9	0.02						
Ar^+		51	46	3.2					
Xe^+	0.14	91	8.7		0.01				
Bz^+			0.63	75	23	1.1			
Na^+			0.09	18	76	6.1	0.06		
An^+				0.06	11	70	13	6.0	

^a r_{max} and R_1 are the locations of the first maximum and minimum in the $S^+ - \text{A}$ radial distribution function. R_2 is the minimum in the $S^+ - \text{C}$ distribution. The two radii R_1 and R_2 are used to define effective first and second coordination shells about the solute. $N_A(R_i)$ and $N_C(R_i)$ are numbers of anions and cations within spheres of radius R_i . ^bValues listed are the percentage occurrence of the anion coordination numbers in the first solvation shell, i.e., instantaneous values of $N_A(R_1)$.

shows radial distribution functions $g_{\text{com}}(r)$ of the center-of-mass positions of cations (C) and anions (A) of the solvent relative to these solutes. Corresponding plots for S^0 and S^- solutes are shown in Figures S1 and S2 in the Supporting Information. The $S^+ - \text{A}$ distributions are particularly simple due to the fact that both the solutes and the anion of ILM2 are spherical. In the case of the smallest solute, Ne^+ , the first maximum in $g_{\text{com}}(r)$ has a value of 24 and the first minimum a value 0.005, indicating a highly ordered first solvation shell.

Table 1 lists several characteristics derived from the radial distribution functions in Figure 2. (See also Table S1, Supporting Information, for corresponding S^0 and S^- data.) r_{\max} and R_1 are the locations of the first maximum and minimum in the S^+ -A distributions, R_2 is the location of the first minimum in the S^+ -C distribution, and $N_A(R_i)$ and $N_C(R_i)$ are anion and cation coordination numbers in the regions bounded by these R_i .

The first solvation shell, as defined by R_1 , contains from 4 (Ne^+) to 14 (An^+) ions, and 2–4 more anions than cations. Out to the first minimum in the S^+ -C distribution (R_2) there are a total of 27 (Ne^+) to 52 (An^+) ion neighbors, again with an excess of 2–4 anions. With the exception of $N_A(R_1)$ these numbers are sensitive to small changes in the choice of radii and are only meant to provide some indication of the shell structure present. Of the solutes studied, only Ne^+ was found to have a particularly well-defined and rigid structure. The relative sizes of Ne^+ and A are such that a tight tetrahedral shell of anions forms around the solute to the total exclusion of cations. As shown in Table 1B, other coordination numbers are found with negligible frequency in the Ne^+ case. In all other cases there is much more variability in the structure, with at least two coordination numbers being prevalent.

As expected, Figure 2 shows that there is a simple evolution of the structure about these spherical solutes as a function of their size. Because it will be used to analyze solvation energies, we consider here the location of the first peak of these radial distribution functions. Specifically, we use the first peak in $g_{\text{com}}(r)$ of whichever species, C or A, approaches most closely to the solute to define an effective solute cavity radius R_{cav} . These cavity radii are plotted in Figure 3 as functions of $R_u + R_v$, where R_u is the solute radius ($\sigma_u/2$) and R_v is the average

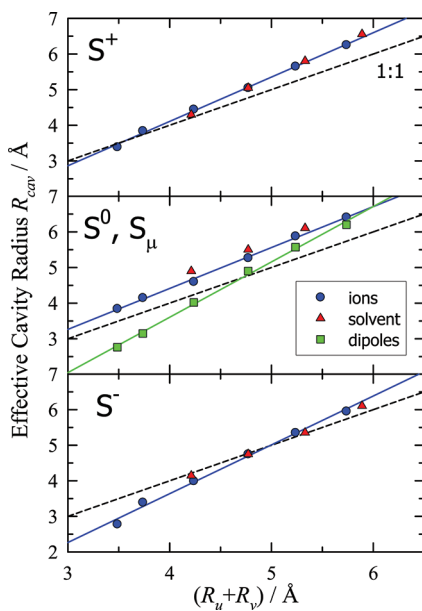


Figure 3. Dependence of the effective cavity radius, defined as the location of the first maximum in $g_{\text{com}}(r)$, as a function of solute + solvent size. R_u is the solute radius $\sigma_u/2$, and R_v is the average solvent site radius (2.24 Å for ILM2). Blue points are data for ionic solutes S^+ , S^0 , and S^- in ILM2 at 350 K. Green points are analogous data for S_μ solutes having a point dipole moment of 5 D instead of a charge. Red points are data from simulations of Bz solutes interacting with solvents of different size at 550 K.

solvent site radius, 2.24 Å for ILM2. The blue circles in Figure 3 show the results for ionic solutes S^+ , S^0 , and S^- in ILM2. For these solutes R_{cav} remains within 15% of $R_u + R_v$ (dashed lines) and increases with solute charge in the order $S^- < S^+ < S^0$. The slopes of the linear fits shown in Figure 3 (1.37, 1.24, and 1.13) follow the reverse order. These variations reflect the different packing available to the C and A components and the absence of electrostriction in the S^0 case. The green points in the middle panel of Figure 3 show results for solutes S_μ in which the charge is replaced by a point dipole moment of 5 D. We note that the slope of the S_μ data (1.55) is much larger than that of the ionic solutes, suggesting a larger structural variation with solute size. Finally, the red points in Figure 3 are from simulations of atomic Bz solutes in modified ILM2 solvents of varying size at 550 K. These systems will be discussed later with respect to solvation energies.

One of the most interesting structural features associated with charged solutes in ionic liquids is the strictly out-of-phase oscillations of cation and anion densities surrounding them. Figure 4 illustrates this behavior for the case of the benzene-like

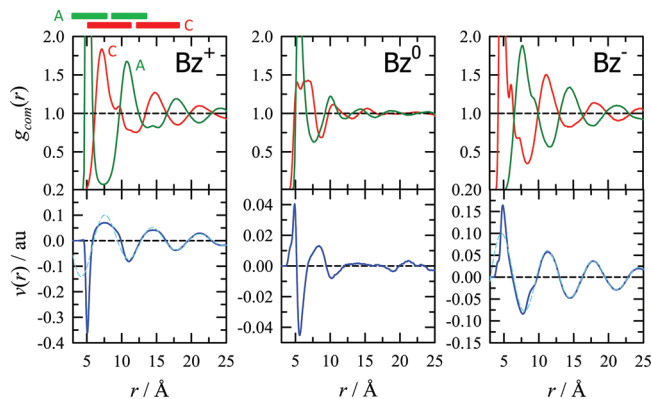


Figure 4. Solvation structure of Bz solutes with charges +1, 0, and -1. (Top) Center of mass radial distribution functions between the solutes and the cations (red) and anions (green) of ILM2. (Bottom) Reaction potential contributions related to charge densities as described in eq 8. Bars above the left-hand panel show lengths equal to the (average) diameters of cations and anions and are meant to indicate the interleaved nature of the cation and anion distributions.

solutes Bz^+ , Bz^0 , and Bz^- . The charge ordering observed with Bz^+ and Bz^- and the other charged solutes is similar to what is observed in the neat solvent itself^{61,60} as well as with spherical solutes in other ionic liquid representations.^{47,49} This structure is most clearly displayed by the charge densities shown in the bottom panels of Figure 4. Rather than plotting charge densities $\rho_q(r)$ directly, we instead plot the “reaction potential contributions”⁷⁶

$$v(r) = 4\pi r \rho_q(r) \quad (8)$$

This terminology reflects the fact that the solvent responds to the solute charge so as to produce an average electrical potential at the solute center, which is given by

$$\langle V \rangle = \int_0^\infty v(r) dr \quad (9)$$

As discussed by Kebinski et al.,⁷⁷ at high ionic strengths $v(r)$ is expected to decay as

$$v(r) \propto \exp(-r/\lambda) \sin(2\pi r/d + \varphi) \quad (10)$$

at large distances. Fits to this functional form (dashed curves in Figure 4) show that such a dependence is observed for all of the charged solutes. Approximately equal values for the periodicity and damping parameters are found for all S^\pm solutes, $d = 6.7 \pm 0.1 \text{ \AA}$ and $\lambda = 11 \pm 1 \text{ \AA}$. These values of d and λ are the same as those found in neat ILM2,⁶¹ indicating that beyond the first full (C+A) solvation shell ($\sim 10 \text{ \AA}$) the structure of the neat ionic liquid is largely unperturbed. Presumably the same is also true of uncharged solutes, but the $v(r)$ functions are not helpful indicators of such structure in this case.

Figure 5 compares the reaction potential contributions observed for the solutes Bz^+ and Bz^- in both ILM2 and in the

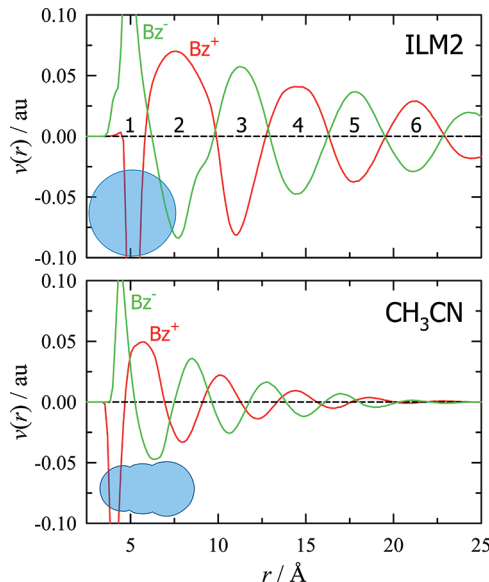


Figure 5. Reaction potential contributions ($v(r)$, eq 8) to solvation of Bz^+ and Bz^- solutes in ILM2 and CH_3CN solvents. Numbers in the top panels label regions bounded by the zero crossings of $v(r)$. Shaded figures show the approximate sizes and locations of A^- anions and CH_3CN in the first solvation shell of the Bz^+ solute.

reference dipolar solvent CH_3CN . This figure illustrates the fact that whereas the charge density response to charged solutes is qualitatively similar in the two solvents, the response is

generally larger and much longer ranged in ILM2 compared to CH_3CN . Fits to eq 10 in the latter case yield $d = 4.3 \text{ \AA}$ and $\lambda = 5.4 \text{ \AA}$. The 2-fold smaller value of λ in CH_3CN compared to ILM2 indicates that charge correlations decay twice as quickly in the dipolar solvent. Part of the difference is a result of the smaller size of CH_3CN compared to the ions of ILM2. However, even when measured in terms of molecular sizes (σ) the correlation length is still nearly twice as large in ILM2 ($\lambda/\sigma = 2.1$) compared to CH_3CN (1.2).

The extent to which different regions of the solvent contribute to the electrostatic solvation energy of a charged solute can be determined by integrating $v(r)$ functions like those shown Figure 5 over r . Doing so shows that the high density of oppositely charged ions in direct contact with the solute (region 1 in Figure 5) produces a potential that is on the order of 10-fold larger than the net reaction potential $\langle V \rangle$. This large overpolarization is quickly reversed by the first shell of like-charged ions in region 2, such that the cumulative effect of regions 1 + 2 is a potential of the wrong sign and still much larger in magnitude than $\langle V \rangle$. This trend is continued with each successive shell of charge density overcompensating for the previous shell such that the integral very slowly converges to the final value of $\langle V \rangle$. This oscillatory nature of $v(r)$ does not allow for a rigorous spatial dissection of the solvation energy. Nevertheless, some perspective on the difference between solvation in ionic and dipolar solvents can be gained by adopting the view that the unsigned areas bounded by the zeros of $v(r)$ represent the relative contributions of various spatial regions to the solvation energy. Using such an analysis we find that in ILM2 about 1/3 of the electrostatic solvation energy of a charged solute comes from the first complete anion + cation shell (regions 1 + 2, out to 9.9 \AA). In the case of these Bz solutes this region contains about 20 ions. The first three cation + anion solvation shells, regions 1–6 (out to 23 \AA), which contains 280 ions, accounts for a total of only $\sim 2/3$ of the solvation energy. The remaining 1/3 comes from a very large number of ions in regions beyond 23 \AA from the solute. In contrast, in the dipolar solvent CH_3CN much more of the solvation energy, roughly 60%, comes from the first complete charge cycle (regions 1 + 2). This initial region (out to 7.0 \AA) contains ~ 16 CH_3CN molecules. After three full charge cycles (regions 1–6, to 15.6 \AA , 190 molecules) 95% of the solvation

Table 2. Solute–Solvent Interaction Energies in ILM2^a

solute	$\langle U_{LJ} \rangle$	$\langle U_{El} \rangle$	$\langle (\delta\Delta U_{El})^2 \rangle$	solute	$\langle U_{LJ} \rangle$	$\langle U_{El} \rangle$	$\langle (\delta\Delta U_{El})^2 \rangle$	solute	$\langle U_{LJ} \rangle$	$\langle (\delta\Delta U_{El})^2 \rangle$
Ne^+	26	-652	1257	Ne^-	14	-632	1402	Ne^0	-6	2016
Ar^+	15	-603	1538	Ar^-	9	-586	1360	Ar^0	-10	1739
Xe^+	-3	-523	1545	Xe^-	-8	-506	1284	Xe^0	-23	1325
Bz^+	-33	-428	1210	Bz^-	-35	-433	1148	Bz^0	-47	1029
Na^+	-58	-372	1093	Na^-	-59	-384	1038	Na^0	-68	865
An^+	-88	-325	975	An^-	-87	-343	936	An^0	-96	734
Ne_μ	15	-193	269	NP	-27	0	1039			
Ar_μ	7	-162	267	IP	-3	-322	742			
Xe_μ	-12	-105	247	$C153(S_0)$	-180	-37	101			
Bz_μ	-42	-62	170	$C153(S_1)$	-184	-81	103			
Na_μ	-65	-42	116							
An_μ	-94	-29	82							

^a LJ and El denote Lennard–Jones and electrostatic interaction energies, respectively, in units of kJ/mol. Fluctuations $\langle (\delta\Delta U_{El})^2 \rangle_0$ refer to electrostatic energy differences $\Delta U_{El} \equiv U_1^{El} - U_0^{El}$ between a given solute state 0 and some reference state 1. Reference states are as follows: for 0 = (S^+ , S^- , and S_μ), 1 = S_0 ; for 0 = S^0 , 1 = S^+ (or S^-); for 0 = NP, 1 = IP and vice versa; and for 0 = $C153(S_0)$, 1 = $C153(S_1)$ and vice versa. Statistical uncertainties in these energies are <1% and in fluctuations 2–5%.

energy is accounted for. These numbers provide some sense of the much larger spatial extent and number of ions/molecules involved in charge solvation in an ionic liquid compared to a dipolar solvent.

3.B. Solvation Energies. Table 2 summarizes average solute–solvent interaction energies and electrostatic energy fluctuations of a variety of solutes in ILM2. Corresponding data in CH₃CN are provided in Table S2 of the Supporting Information. For ionic solutes the majority of the solute–solvent interaction energy U comes from electrostatic interactions, U_{El} . Even for the largest atomic solute An, whose Lennard–Jones parameters are meant to mimic those of anthracene, only 20% of the interaction with the ionic liquid results from nonelectrostatic sources (U_{LJ}). For the smallest ionic solutes Ne $^{\pm}$ and Ar $^{\pm}$, Lennard–Jones interactions are slightly unfavorable, $\langle U_{\text{LJ}} \rangle > 0$, as a result of electrostriction. While the same is true in the case of the smallest dipolar solutes ($\mu = 5$ D), for the larger members of the S_{μ} series a much larger proportion of the solvation energy results from Lennard–Jones interactions terms. Finally, in the polyatomic solute C153 only 17% (S_0) or 31% (S_1) of the interaction with ILM2 comes from electrostatics. Comparison of the data in Tables 2 and S2, Supporting Information, shows that the energetic breakdown is very similar in CH₃CN and ILM2. In the remainder of this work we focus exclusively on the electrostatic portion of the problem.

Figure 6 shows a comparison of the electrostatic solvation energies of all solutes studied in ILM2 and CH₃CN. Similar to

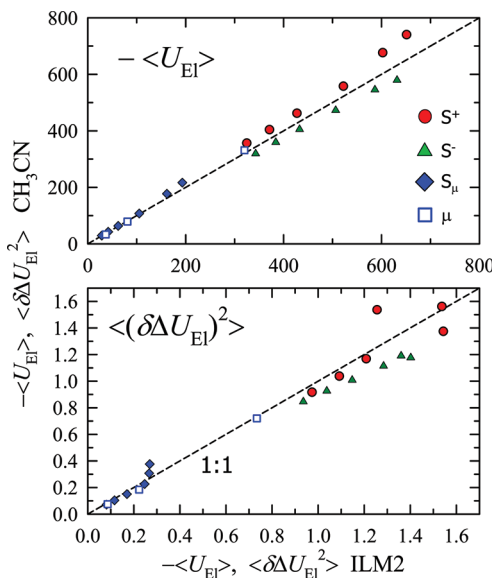


Figure 6. Comparison of electrostatic solvation energies $\langle U_{\text{El}} \rangle$ and fluctuations $\langle (\delta U_{\text{El}}^2) \rangle$ in ILM2 and CH₃CN. S⁺, S⁻, and S_{μ} are the single-site solutes Ne–An, and μ denotes the diatomic IP and polyatomic C153 solutes. Units of $\langle U_{\text{El}} \rangle$ are kJ/mol, and units of $\langle (\delta U_{\text{El}}^2) \rangle$ are 10^3 kJ² mol⁻².

what has been noted in previous simulations,^{29,32,47} we find the electrostatic solvation energies (top) in ILM2 are close to those in the dipolar solvent CH₃CN. For dipolar solutes, the near equality of these energies is remarkable with the difference between the energies in the two solvents being less than 5% in most cases. This similarity is in accord with experimental solvatochromic measurements, which indicate that ionic liquids like [Im₄₁][PF₆] have polarities comparable to those of highly

polar conventional solvents such as CH₃CN, methanol, and dimethylsulfoxide.^{19,78,10} In the case of ionic solutes, Figure 6 shows that cation solvation is slightly more favorable in CH₃CN relative to ILM2 and anion solvation slightly less favorable. Nevertheless, electrostatic solvation energies in the two solvents fall within 10% of one another in nearly all cases studied.

We note that the electrostatic solvation energies computed in ILM2 are similar to those previously reported in simulations using more detailed ionic liquid representations. For example, Lynden-Bell⁴⁹ simulated a series of spherical solutes having unit charge much like our S⁺ series in a model of [Im₁₁][PF₆]. She reported values of electrostatic solvation energies versus solute size which are uniformly ~15% more negative than ours. Comparing our values of $\langle U_{\text{El}} \rangle$ for the ion pair (IP) solute of Shim and Kim we find their energies to be ~16% and ~32% more negative than ours in models of [Im₂₁][Cl] and [Im₂₁][PF₆], respectively. Such differences are expected due to the somewhat higher ion densities of the ionic liquids in these previous studies and, more importantly, due to the reduced ion charges ($\pm 0.78e$) of ILM2.

Also listed in Table 2 and shown in the bottom panel of Figure 6 are the fluctuation magnitudes $\langle (\delta U_{\text{El}}^2) \rangle$. As discussed in section 2, these fluctuations in the differences between the electrostatic energies of two solute charge states “0” and “1”, $\Delta U_{\text{El}} \equiv U_1^{\text{El}} - U_0^{\text{El}}$, are of interest with respect to linear response predictions and Marcus-type descriptions of charge-transfer energetics. With the exception of the C153 solute, the perturbations 0 \leftrightarrow 1 involve states having either “full” (S⁺, S⁻, S_{μ} , IP) or no (S⁰, NP) electrostatic interactions with the solvent, which means that in many cases $\Delta U_{\text{El}} = \pm U_{\text{full}}^{\text{El}}$ and $\langle (\delta U_{\text{El}}^2) \rangle = \langle (\delta U_{\text{full}}^{\text{El}})^2 \rangle$. Several groups^{32,33,47,79,45} have already examined the applicability of Marcus theory for describing solvation free energies in simulations of ionic liquids (and CH₃CN). We do not study this problem in detail but merely note here that our observations on the ILM2 model liquid are similar to what these workers found using more realistic representations. We find that the probability distributions of ΔU_{El} observed in equilibrium simulations are Gaussian functions to within uncertainties. As illustrated by the examples in Figure S3, Supporting Information, the free energy profiles they imply are parabolic out to energies of $10k_{\text{B}}T$ and well described by

$$G(\Delta U_{\text{El}}) \cong G_0 + \frac{1}{2}k_s(\Delta U_{\text{El}} - \langle \Delta U_{\text{El}} \rangle)^2 \quad \text{with} \\ k_s = \frac{k_{\text{B}}T}{\langle (\delta U_{\text{El}}^2) \rangle} \quad (11)$$

The fact that values of the solvation force constants k_s differ in different charge states of a given solute (for example Ne⁺, Ne⁰, Ne⁻) means the solvation response is not strictly linear and that eq 3 cannot be accurate for sufficiently large fluctuations.

Some measure of the departure from linear behavior is reported in Table 3. In this table we list the percentage errors incurred in using fluctuation magnitudes $\langle (\delta U_{\text{El}}^2) \rangle$ to predict the energy differences between uncharged (S⁰ and NP) and their fully charged (S⁺, S⁻, S_{μ} and IP) counterparts. (In the case of the C153 solute the difference considered is between the ground electronic state S_0 ($\mu = 6.2$ D) and an excited state S_1 ($\mu = 13.9$ D)⁶⁴). The calculations use eq 3 with $t = 0$ and eq 1 to predict the solvation energy difference between charge states 0 and 1 via

Table 3. Errors in Linear Response Estimates of Solvation Energies^a

	$\Delta = S^0 \leftrightarrow S^+$		$\Delta = S_0 \leftrightarrow S^-$		$\Delta = S_0 \leftrightarrow S_\mu$	
	S^0 , %	S^+ , %	S^0 , %	S^- , %	S^0 , %	S_μ , %
Ne	5	-34	11	-25	21	-52
Ar	-2	-14	3	-21	3	-43
Xe	-14	0	-8	-14	-20	-19
Bz	-20	-6	-16	-5	-24	-6
Na	-23	-2	-20	-1	-27	-5
An	-25	-1	-24	3	-28	-2
	$\Delta = NP \leftrightarrow IP$		$\Delta = C153 S_0 \leftrightarrow S_1$			
NP	IP		S_0	S_1		
	+11%	-21%	2%	4%		

^aHeadings $\Delta = 0 \leftrightarrow 1$ indicate the charge transformation considered, numerical values are percentage errors in the linear response estimates $\langle \Delta U_{\text{El}} \rangle_0^{\text{eq}} - \langle \Delta U_{\text{El}} \rangle_1^{\text{eq}} \cong \langle (\delta \Delta U_{\text{El}})^2 \rangle_0^{\text{eq}} / k_B T$ or $\langle (\delta \Delta U_{\text{El}})^2 \rangle_1^{\text{eq}} / k_B T$ based on fluctuations measured in both end points of the transformation. Negative values indicate that the linear response estimates underestimate the magnitude of the energy difference. Uncertainties in these comparisons are on the order of 2–5%.

$$\langle \Delta U_{\text{El}} \rangle_0^{\text{eq}} - \langle \Delta U_{\text{El}} \rangle_1^{\text{eq}} \cong \langle (\delta \Delta U_{\text{El}})^2 \rangle_0^{\text{eq}} / k_B T \quad (12)$$

The results in Table 3 indicate that such linear response estimates are relatively inaccurate for the smallest single-site solutes. Using fluctuations observed in the fully charge state (S^+ , S^- , S_μ) provides predictions of energy differences that are within the statistical uncertainties in the case of the largest solutes Na and An. In contrast, the smaller fluctuations measured in simulations of the S^0 solutes yield predictions that significantly underestimate the energy differences observed.

One goal of these simulations was to suggest simple relationships for estimating electrostatic solvation energies in ionic liquids. In conventional solvents one typically relies on dielectric continuum estimates, for example, the expressions

$$\langle U_q \rangle = -\frac{q^2}{a} \left(1 - \frac{1}{\epsilon_r} \right) \quad (13a)$$

and

$$\langle U_\mu \rangle = -\frac{2\mu^2}{a^3} \left(\frac{\epsilon_r - 1}{2\epsilon_r + 1} \right) \quad (13b)$$

for the electrostatic energies of a point charge q or point dipole moment μ centered in a spherical cavity of radius a in a medium having relative permittivity ϵ_r . We follow Lynden-Bell⁴⁹ and use eqs 13a and 13b with $\epsilon_r = \infty$ to view the observed electrostatic energies in terms of the effective cavity radii they imply

$$R_{\text{El}}^q = -\frac{q^2}{\langle U_{\text{El}} \rangle} \quad (14a)$$

and

$$R_{\text{El}}^\mu = \left(-\frac{\mu^2}{\langle U_{\text{El}} \rangle} \right)^{1/3} \quad (14b)$$

In Figure 7 we compare these effective cavity radii to two structural parameters, R_{cav} defined in terms of the first peak in the solute–solvent radial distribution functions, and R_u the bare solute radius ($\sigma_u/2$). As illustrated in Figure 7, the effective

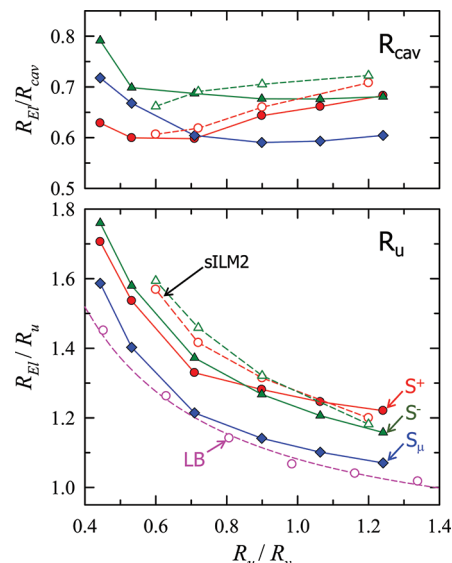


Figure 7. Comparison of geometric radii (R_{cav} , R_u , and R_v) and effective radii deduced from electrostatic solvation energies (R_{El}) using the continuum relations eqs 14a and 14b. R_{cav} is the effective solute radius, defined as the location of the first maximum in $g_{\text{com}}(r)$, R_u is the solute radius ($\sigma_u/2$), and R_v is the average ion radius. Filled points and solid lines are data in ILM2 at 350 K; open symbols and dashed lines are data in other ionic liquid models. Points labeled “sILM2” are data for S^+ (circles) and S^- (triangles) solutes in scaled versions of ILM2 at 550 K, and those labeled “LB” are solutes similar to S^+ in $[\text{Im}_{11}][\text{PF}_6]$ reported by Lynden-Bell.⁴⁹ The smooth curve through these latter data is the fit $R_{\text{El}} = 0.79R_u + 0.29R_v$.

solute sizes deduced from eqs 14a and 14b in all cases fall between the two structural estimates, i.e., $R_{\text{cav}} > R_{\text{El}} > R_u$. Although one might have expected use of R_{cav} would provide the best estimates of solvation energies, the bare solute radius R_u is the better choice, especially at larger solute sizes where R_{El}/R_u appears to approach unity. Similar trends with solute size are also found in the dipolar solvent CH_3CN (Figure S4, Supporting Information), where it is likewise found that R_u appears to be more simply related to solvation energy.

To generalize the results obtained with ILM2 we also examined solvation of Bz^+ and Bz^- solutes in “scaled” versions of ILM2 wherein the linear dimensions of the solvent ions were scaled over the range $\lambda = 0.75–1.5$. To avoid the sluggish dynamics observed in some of these scaled liquids, simulations were run at 550 K. The open symbols and dashed lines labeled “sILM2” in Figure 7 are results obtained in these other ionic liquids. The points at $R_u/R_v \approx 0.9$ are for $\lambda = 1.0$, i.e., they correspond to ILM2 at the higher temperature of 550 K. The ~3% difference in R_{El} (or $\langle U_{\text{El}} \rangle$) compared to the 350 K data indicates how little sensitive ion solvation energies are to temperature variations in ionic liquids. This insensitivity exists despite the fact that the density of ILM2 is ~10% lower at 550 K relative to 350 K. Also shown in Figure 7 are the results obtained by Lynden-Bell for ions comparable to our S^+ solutes in a model of $[\text{Im}_{11}][\text{PF}_6]$ at 450 K.⁴⁹ The solute size dependence is quite similar to what we observe, but as mentioned before, solvation energies are uniformly larger and thus effective radii smaller by ~15% due to the difference in charge densities of the two ionic liquid models employed.

In all cases, solvation energies of spherical solutes can be reasonably represented using effective electrostatic radii of the form $R_{\text{El}} \cong aR_u + bR_v$ (The smooth curve through the Lynden-

Bell data shows an example of such a representation.) Ionic solutes in ILM2 and scaled ILM2 solvents are represented with an average absolute error of <3% and a maximum error of 7% with $a = 0.86$ and $b = 0.40$. The entire collection of ion solvation data in Figure 7, including the Lynden-Bell data, are represented with an average of 7% and a maximum of 15% using $a \cong 0.8$ and $b \cong 0.4$. This latter correlation should provide first estimates of electrostatic ion solvation energies in real systems based upon solute and solvent size alone. Dipolar solvation energies (S_μ , blue diamonds) can be represented in a similar fashion. We note that the polyatomic dipolar solutes IP and $S_1\text{-C}153$ (not plotted) fall far from the correlation established by the spherical S_μ solutes, while $S_0\text{-C}153$ is close. (Coordinates $(R_u/R_v, R_{\text{EL}}/R_u)$ of IP, $S_1\text{-C}153$, and $S_0\text{-C}153$ are (0.89, 1.48), (1.38, 1.02), and (1.38, 1.33), respectively.) Given the greater sensitivity of continuum estimates to solute size and shape in the case of dipolar solutes (eq 14b) it seems unlikely that any simple spherical point dipole model will provide accurate estimates of solvation energies for neutral polyatomic solutes in ionic liquids. The same is also true in conventional solvents like CH_3CN .

3.C. Solvation Dynamics. We now consider the time dependence of the electrostatic component of solvation. We begin with the equilibrium time correlation functions (tcfs), $C_\Delta(t)$, which describe fluctuations in the electrostatic energy difference $\delta\Delta U_{\text{el}}$ as defined in eq 4. These tcfs are the linear response estimates for the nonequilibrium response $S_\Delta(t)$ to step-function perturbations of the solute charge distribution. Figure 8 shows examples of such functions corresponding to

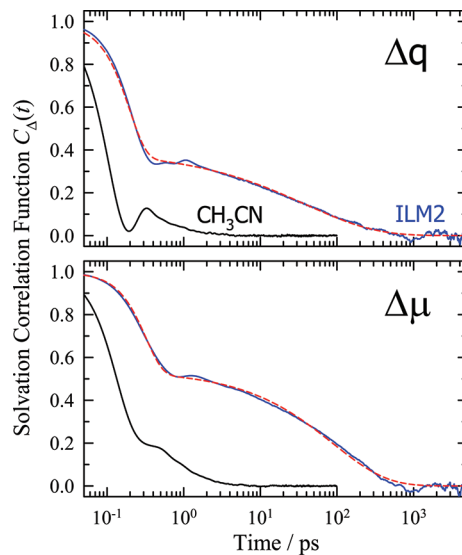


Figure 8. Solvation time correlation functions $C_\Delta(t)$ of the Bz^0 solute in ILM2 (350 K) and CH_3CN (298 K). (Top) Functions associated with a charge perturbation and (bottom) a dipole perturbation. Solid curves are the simulated correlation functions and dashed red curves fits to these functions using eq 15.

charge (Δq) and dipole ($\Delta \mu$) perturbations of an immobile Bz^0 solute in ILM2 (350 K) and CH_3CN (298 K). Although there is an appreciable difference in time scale, the tcfs observed in ILM2 and CH_3CN share some common features. In both solvents, $C_\Delta(t)$ functions consist of a subpicosecond component which accounts for a substantial fraction of the overall decay, some oscillatory behavior at intermediate times, followed finally by a slow component in the picosecond time

domain. Correlation functions corresponding to a charge perturbation decay more quickly than do those corresponding to dipolar perturbations in both solvents. Such differences have been well studied in the case of dipolar liquids^{80,81} where they have been shown to reflect the different spatial range probed by different solute multipoles.^{79,80} The same explanation also seems to apply in the case of ionic liquids.⁸ With few exceptions (for example, Ne^+ , see below) one can represent such $C_\Delta(t)$ functions with reasonable accuracy using a Gaussian plus stretched exponential representation

$$C_\Delta(t) \cong f_G \exp\left(-\frac{1}{2}\omega_G^2 t^2\right) + (1 - f_G)\exp\{-(t/\tau)^\beta\} \quad (15)$$

The dashed curves in Figure 8 illustrate the quality of fits to this functional form typically found for uncharged and dipolar solutes. Values of the exponent β are in the range 0.4–0.6, indicating that the slow component is broadly distributed in time. As noted in the Introduction, this distributed nature of the slow solvation component has long been recognized from experimental studies as one of the most distinctive features of solvation in ionic liquids.

The variety of $C_{\Delta q}(t)$ functions observed with single-site solutes are shown in Figure 9. In the case of small solutes,

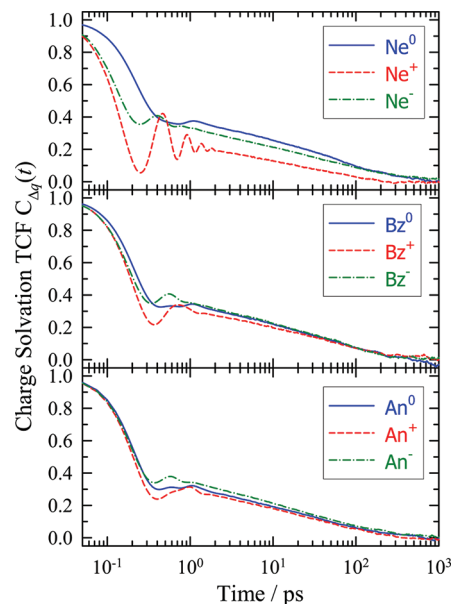


Figure 9. Solvation time correlation functions $C_{\Delta q}(t)$ associated with charge perturbations in Ne, Bz, and An solutes in ILM2 at 350 K.

typified by Ne in the top panel, the structural differences as a function of solute charge discussed in section 3.A give rise to substantial differences in both the fast and the slow components of solvation. For example, the much looser first solvation shell of Ne^0 compared to Ne^+ and Ne^- produces a much slower initial decay of $C_{\Delta q}(t)$. The pronounced oscillations in the Ne^+ tcf are due to vibrations of anions in its highly structured first solvation shell. The oscillations in Ne^- are much more subtle than those of Ne^+ , primarily because the polyatomic nature of the cations in its first solvation shell undermines the coherence of the first-shell vibrations. Finally, in the uncharged solute Ne^0 , the oscillations are difficult to discern. In general, we find that marked oscillations in $C_{\Delta q}(t)$ are only present in highly symmetric solutes having high charge

densities. As will be seen later, even the single oscillations found in the $C_{\Delta q}(t)$ in Figure 9 are absent in polyatomic solutes of the sort used in experiment. It can also be seen in Figure 9 that the influence of solute charge is considerably smaller in the case of larger solutes like Bz and An, and in these cases the details of solvation structure are relatively unimportant. In the remainder of this work we focus either on uncharged solutes or on charged Bz solutes in order to probe dynamics largely independent of specific structural effects of the sort found in Ne^{\pm} .

Figure 10 illustrates how S^0 correlation functions depend upon solute (Figure 10a) and temperature (Figure 10b). In the

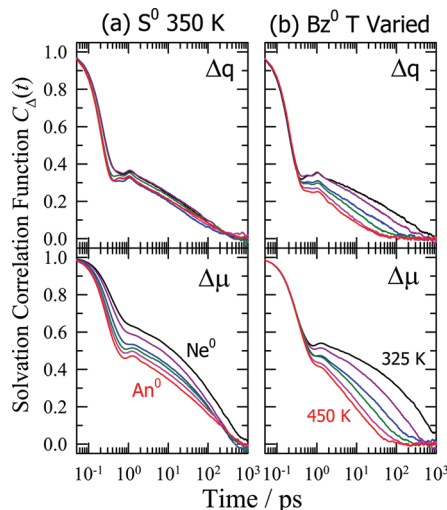


Figure 10. Solvation time correlation functions $C_{\Delta}(t)$ of immobile uncharged solutes in ILM2. (a) Solutes of varying size: Ne^0 , Ar^0 , Xe^0 , Bz^0 , Na^0 , and An^0 at 350 K. (b) Bz^0 at temperatures of 325, 350, 375, 400, 425, and 450 K. (Top) Functions associated with charge perturbations and (bottom) dipole perturbations.

case of dipole perturbations, there is a clear trend of increasingly rapid relaxation as solute size increases. This trend is most clear in the solvation frequency

$$\omega_s^2 \equiv - \left(\frac{d^2 C_{\Delta}(t)}{dt^2} \right)_{t=0} = \frac{\langle (\Delta U_{\text{EI}})^2 \rangle}{\langle (\delta \Delta U_{\text{EI}})^2 \rangle} \approx \omega_G^2 \quad (16)$$

and in the amplitude of the Gaussian component, f_G . These and other features of the $C_{\Delta}(t)$ functions of a variety of solutes are summarized in Table 4. The solvation frequency characterizes the inertial component of the solvation response. In ILM2, ω_s lies in the range 5–6 ps^{-1} for ionic perturbations and 3–4 ps^{-1} for dipolar perturbations. These values are uniformly smaller than the corresponding frequencies in CH_3CN by a factor of 2.6 ± 0.2 for the tabulated comparisons. Given that the fluctuation magnitudes $\langle (\delta \Delta U_{\text{EI}})^2 \rangle$ and thus force constants (k_s , eq 11) are comparable in the two solvents, this difference in frequencies results from differences in the “solvation mass”⁶⁹ $m_s = k_s / \omega_s^2$. The fact that $m_s(\text{ILM2}) / m_s(\text{CH}_3\text{CN}) \approx 6.8$ is much larger than the actual mass ratio $m(\text{C}_6\text{A}) / m(\text{CH}_3\text{CN}) = 3.5$ reflects a change in the mechanism of inertial solvation from being nearly all rotational in CH_3CN ⁸¹ to being mainly translational in ILM2.

The S^0 data in Table 4 indicate that the solvation frequency increases systematically with solute size, with the effect being much larger (49%) for dipolar compared to charge (12%).

perturbations. For charge perturbations, the amplitude of the Gaussian component, f_G , is independent of solute size and no systematic variation of the integral time associated with the slow solvation component $\langle \tau \rangle_{\text{str}}$ can be discerned. Dipolar perturbations, on the other hand, show a clear increase in the relative contribution of the fast component, f_G , and a slight increase in $\langle \tau \rangle_{\text{str}}$ with increasing size for solutes larger than Ar. Finally, we note that the stretching exponent β is smaller for ionic perturbations, indicating a more distributed character of the long solvation component in the charge versus dipole perturbations.

Temperature-dependent $C_{\Delta}(t)$ functions of the Bz^0 solute are shown in Figure 10b. As illustrated here, whereas the amplitude of the Gaussian component increases systematically with increasing temperature, the solvation frequency varies surprisingly little between 325 and 450 K. For charge and dipole perturbations ω_s decreases by ~5% and ~1% with increasing temperature. Although molecular velocities increase by ~18% between 325 and 450 K, which acts to increase the solvation frequency, this effect is counterbalanced by the diminished amplitude of the fluctuations caused by the 10% decrease in solvent density over this temperature range. In contrast to these minor changes in the fast solvation component, the time scale of the slow component of $C_{\Delta}(t)$ changes markedly with temperature.

The overall correlation times of the $C_{\Delta}(t)$ tcfs are plotted versus solvent viscosity η/T in Figure 11. (Viscosities are from the simulations of neat ILM2 described in ref 61.) As seen in this figure, the times associated with dipole solvation are consistently about 5-fold larger than charge solvation times. Both times are reasonably fit by power laws, $\langle \tau_s \rangle \propto (\eta/T)^p$, with powers p close to unity. Correlations of similar quality are obtained using the times associated only with the slow solvation component or using η rather than η/T . Also shown schematically in Figure 11 are results from experimental measurements on C153.¹⁰ The dashed line represents a correlation obtained with 15 assorted ionic liquids near to room temperature.⁸² The same sort of scaling with η/T or η has been observed in a number of other experimental^{83,7,18,17} and theoretical⁸⁴ studies. This connection between solvation time and viscosity is another characteristic feature of ionic liquid solvation which appears to be captured by these simulations. We note that rotational and translational diffusion times of the ions of ILM2 are also nearly proportional to the hydrodynamic factor η/T .⁶¹ While no particular mechanism can be inferred from this dependence, it is clear that the slow component of solvation involves motions coupled to hydrodynamic modes of the solvent.

A comparison of the solvation correlation function simulated for C153 in ILM2 and the solvation response $S_{\Delta}(t)$ observed experimentally in $[\text{Im}_{41}][\text{PF}_6]$ ⁸ is provided in Figure 12. The experimental data were recorded at 293 K, whereas the simulations were run at 350 K and extrapolated to 293 K (dashed curve) using the temperature dependence observed for the Bz^0 solute.⁸⁵ We resorted to this indirect approach because at 293 K runs of 500 ns duration did not produce $C_{\Delta}(t)$ functions that were well converged. As shown in Table 4, the characteristics of $C_{\Delta}(t)$ associated with the $S_0 \leftrightarrow S_1$ charge redistribution in C153 tend to be intermediate between those of charge and dipole perturbations in the larger single-site solutes. The simulated amplitude of the solvation response, calculated from differences in $\langle \Delta U_{\text{EI}} \rangle$ in the S_1 and S_0 solutes, is 2840 cm^{-1} , which may be compared to an observed value of

Table 4. Characteristics of Equilibrium Solvation TCFs $C_\Delta(t)$ ^a

solute	Δ	$\langle(\delta\Delta U_{\text{El}})^2\rangle/(k\text{J/mol})^2$	ω_s/ps^{-1}	f_G	ω_G/ps^{-1}	τ_0/ps	β	$\langle\tau\rangle_{\text{str}}/\text{ps}$	$\langle\tau_s\rangle/\text{ps}$
ILM2									
Ne ⁰	Δq	2016	5.0	0.60	6.3	40	0.51	78	28
Ar ⁰	Δq	1739	5.1	0.59	6.4	45	0.49	93	33
Xe ⁰	Δq	1325	5.5	0.63	7.0	27	0.49	58	21
Bz ⁰	Δq	1029	5.6	0.61	7.1	39	0.48	85	24
Na ⁰	Δq	865	5.6	0.58	7.2	26	0.39	94	34
An ⁰	Δq	734	5.7	0.62	7.3	36	0.44	93	32
Bz ⁺	Δq	1210	6.4	0.65	8.6	39	0.46	92	28
Bz ⁰	Δq	1029	5.6	0.61	7.1	39	0.48	85	24
Bz ⁻	Δq	1148	6.4	0.56	8.6	27	0.45	69	22
Ne ⁰	$\Delta\mu$	269	2.5	0.33	3.4	127	0.56	210	129
Ar ⁰	$\Delta\mu$	267	2.8	0.38	3.5	91	0.64	126	72
Xe ⁰	$\Delta\mu$	247	3.2	0.45	4.0	88	0.67	117	59
Bz ⁰	$\Delta\mu$	170	3.4	0.46	4.4	89	0.62	127	63
Na ⁰	$\Delta\mu$	116	3.6	0.47	4.6	82	0.55	140	66
An ⁰	$\Delta\mu$	82	3.8	0.47	4.8	67	0.50	135	63
NP	$\Delta\{q_i\}$	1039	3.8	0.45	5.1	29	0.55	50	29
IP	$\Delta\{q_i\}$	742	5.9	0.61	7.9	71	0.53	129	50
C153 S ₀	$\Delta\{q_i\}$	35	4.4	0.48	5.7	67	0.59	103	59
C153 S ₁	$\Delta\{q_i\}$	35	4.2	0.45	5.7	79	0.51	150	70
CH ₃ CN									
Bz ⁰	Δq	814	14	0.89	15.7	1.00	1.00	1.00	0.18
Bz ⁰	$\Delta\mu$	151	10	0.72	10.8	0.92	1.00	0.92	0.35
NP	$\Delta\{q_i\}$	1043	11	0.80	12.1	1.06	1.00	1.06	0.29
IP	$\Delta\{q_i\}$	725	14	0.80	16.3	1.29	1.00	1.29	0.34
C153 S ₀	$\Delta\{q_i\}$	31	12	0.68	13.6	0.84	0.88	0.90	0.37
C153 S ₁	$\Delta\{q_i\}$	30	12	0.67	13.9	0.79	0.87	0.84	0.38

^a Δ indicates the type of perturbation considered, $\langle(\delta\Delta U_{\text{El}})^2\rangle$ is the fluctuation magnitude assuming perturbations of size $\Delta q = 1e$, $\Delta\mu = 5 \text{ D}$, and distributed charge perturbations $\Delta\{q_i\}$ corresponding to NP \leftrightarrow IP and C153 S₀ \leftrightarrow S₁ transitions. ω_s is the solvation frequency defined by eq 16, obtained by fitting only the initial portion of $C_\Delta(t)$. f_G , ω_G , τ_0 , and β are parameters of fits to eq 15. $\langle\tau\rangle_{\text{str}}$ is the integral time associated with the stretched exponential component, and $\langle\tau_s\rangle$ is the overall correlation time of $C_\Delta(t)$. Estimated uncertainties in ω_s , f_G , and β are $\leq 10\%$ and in $\langle\tau_s\rangle$ between 15% and 30%.

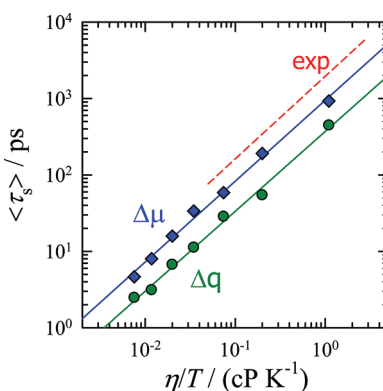


Figure 11. Integral times of $C_\Delta(t)$ charge (circles) and dipole (diamonds) perturbations in the Bz⁰ solute plotted versus solvent viscosity (η/T). Lines are the fits $\langle\tau_{\Delta q}\rangle = 180(\eta/T)^{1.05}(\Delta q)$ and $\langle\tau_{\Delta\mu}\rangle = 948(\eta/T)^{1.06}(\Delta\mu)$. Dashed line labeled "exp" shows the fit of experimental measurements with the probe C153.^{10,82}

2200 cm⁻¹.¹⁰ As indicated in the table inset to Figure 11, the simulated C153 curves exhibit comparable values of ω_G and β to what is measured experimentally, indicating that the simulations properly capture the time scale associated with the inertial solvation component and the highly distributed character of the diffusive component of the solvation response.

The main source of disagreement between simulation and experiment lies in the amplitude of the fast solvation

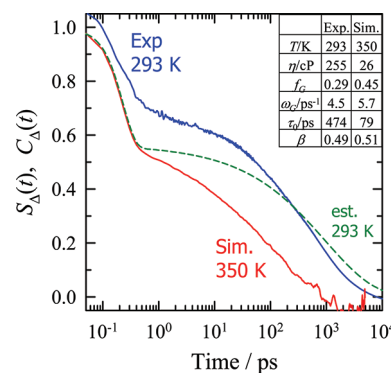


Figure 12. Comparison of the solvation response function $S_\Delta(t)$ of C153 at 293 K⁸ (blue curve) with the simulated solvation correlation function $C_\Delta(t)$ of C153 (S₁) at 350 K (red). Inset table lists parameters of fits of these functions to eq 15. Curve labeled "est. 293 K" is $C_\Delta(t)$ estimated based on extrapolation of the temperature dependence observed with the Bz⁰ solute⁸⁵ (for this estimate the fit parameters are $f_G = 0.44$, $\omega_G = 6.1$, $\tau_0 = 970 \text{ ps}$, $\beta = 0.49$).

component, f_G , which is significantly overestimated by the simulations (45% vs 29%). As seen in Table 4, f_G tends to be smaller for dipolar than for charge perturbations. The value of f_G simulated for C153 is similar to the values of the dipole perturbations in single-site solutes, all of which are larger than the experimental value. Most prior simulations of solvation dynamics in ionic liquids employed small atomic⁵⁰ or

diatomic^{30,54,35,41,46} solutes and predicted inertial components of solvation greater than 50%. Only the simulations of Kobrak^{38,40} which employed a realistic polyatomic solute (C153) showed much smaller inertial components, $f_G = 13\text{--}24\%$.^{38,40} This large difference suggested that the solute representation was to blame for the exaggerated importance of the fast component in simulation relative to experiment. In the present case it must be a shortcoming of the solvent model that is responsible for the disagreement. Given the simplifications inherent in ILM2 it is probably unreasonable to expect a quantitative match with experiment. Nevertheless, the level of agreement shown in Figures 11 and 12 is sufficient to suggest that the simulations capture the essential features of the dynamics being measured experimentally.

Before examining the ion motions underlying $C_\Delta(t)$ or $S_\Delta(t)$ we first consider two additional aspects of these functions. The first is the effect of solute motion. With the exception of the C153 solute, all of the results shown in Figures 8–11 and Table 4 were obtained with immobile solutes in order to focus on the solvent contributions to solvation dynamics. However, especially for small or light solutes, one would expect solute motions could significantly increase the rate of solvation. Figure 13 illustrates the extent of this effect in C153 and the diatomic

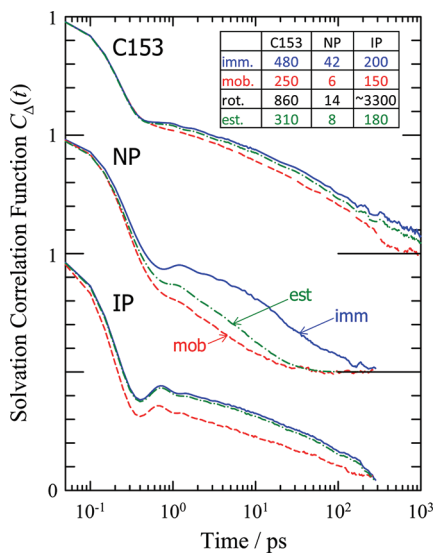


Figure 13. Comparison of solvation correlation functions $C_\Delta(t)$ of immobile (solid blue curves) and mobile (dashed red) solutes in ILM2 (350 K). Green dash-dot curves are estimates of the effect of solute rotation based on eq 17. For clarity, the curves for the NP and C153 solutes are shifted vertically by 0.5 and 1.0, respectively. Inset table lists integral times (in ps) associated with the long decay components of the immobile (imm.) and mobile (mob.) $C_\Delta(t)$ functions, first-rank rotational correlation function of the solute dipole vector (rot.), and estimated $C_\Delta(t)$.

solutes NP and IP. In the case of C153 there is no detectable effect of solute motion on the inertial portion of $C_\Delta(t)$, whereas the integral time of the slow component (see inset table to Figure 13) is reduced by roughly a factor of 2. In the case of the IP solute, solute motion appears to primarily increase the speed and amplitude of the inertial response while causing only a small change in the slow component. Finally, in the case of the NP solute, there is both a speed-up of the fast solvation component and a dramatic (7-fold) change in the integral time of the slow component. Previous simulations of solvation in

CH_3CN and methanol⁸⁰ showed that the effect of solute rotational motion on solvation tcfs corresponding to a dipolar perturbation could be approximately estimated from

$$C_\Delta^{\text{mob}}(t) \cong C_\Delta^{\text{imm}}(t) \cdot C_{\text{rot}}(t) \quad (17)$$

where $C_\Delta^{\text{imm}}(t)$ is the solvation tcf in the absence of solute motion and $C_{\text{rot}}(t) = \langle \hat{u} \cdot \hat{u}(t) \rangle$ is the tcf of a unit vector \hat{u} in the difference dipole direction. The extent to which this approximation explains the differences observed here is shown by the curves labeled “est” in Figure 13. The inset table also lists integral times of $C_{\text{rot}}(t)$ (“rot”) and of the long component of the estimated $C_\Delta^{\text{mob}}(t)$. This comparison suggests that rotational solute motions account for a significant portion of the differences between $C_\Delta^{\text{mob}}(t)$ and $C_\Delta^{\text{imm}}(t)$. Rotation of C153 involves a negligible inertial component (<2%), and the correlation time of $C_{\text{rot}}(t)$ is about twice the integral time of the slow solvation component in $C_\Delta^{\text{imm}}(t)$. In this case eq 17 predicts a negligible effect on the fast solvation dynamics but a significant enhancement in the speed of the slow component. This predicted enhancement is, however, not as large as what is observed. For the IP solute, $C_{\text{rot}}(t)$ exhibits a modest inertial component (~8%) but the rotational correlation time is much longer than the solvation time, >3 ns versus 200 ps for the slow solvation component. (Such slow rotation of the IP solute has been reported in several prior simulations.^{46,56}) In this case, rotation is predicted to have small effects on both the short- and long-time dynamics of $C_\Delta(t)$. The observed effect of solute motion is much larger than predicted. Finally, rotation of the NP solute is much more rapid than in the other two solutes: $C_{\text{rot}}(t)$ reaches 0.5 in 7 ps, and the rotational correlation time is only 14 ps. In this case solute rotation is predicted to dramatically increase the rate of solvation, and eq 17 accounts for most but not all of this increase. In all three cases the residual rate enhancements beyond those predicted by eq 17 might reasonably be attributed to the effects of solute translation. The increases in solvation frequencies, 7–8% in the NP and IP solutes, are undoubtedly due to solute translation. Whether the differences between the long-time constants (inset table) based on eq 17 estimates and those measured for the fully mobile solutes are a result of probe translation is less clear.

We note that Kashyap and Biswas recently⁸⁶ modeled the effect of diffusive solute rotation and translation theoretically. They found that even for large solutes like C153 solute motions can cause a significant increase in the rate of solvation. In cases where the dipolar nature of solvent ions is unimportant, they concluded that rotation is the primary solute motion effective for relaxing the solvation energy. The simulations presented here are generally consistent with these theoretical predictions. Further simulations will be required to more fully explore the effects of solute motion on the solvation response. For now, we would only like to emphasize the fact that solute motions may play a more important role in ionic liquid solvation than has been appreciated in the case of dipolar solvation.

Another aspect of interest, examined in Figure 14, is the linearity of the solvation response. In this figure we compare the linear response estimates $C_\Delta(t)$ discussed thus far to the nonequilibrium response $S_\Delta(t)$ observed after the $S_0 \rightarrow S_1$ transition in C153 (top) and the four charge jumps $\text{Bz}^- \leftrightarrow \text{Bz}^0 \leftrightarrow \text{Bz}^+$ (bottom panels). In the case of C153, the observed nonequilibrium dynamics are well predicted by the dynamics of fluctuations in ΔU_{El} observed in equilibrium with either the S_0 or the S_1 state. As reported previously in dipolar solvents,⁸⁷ we

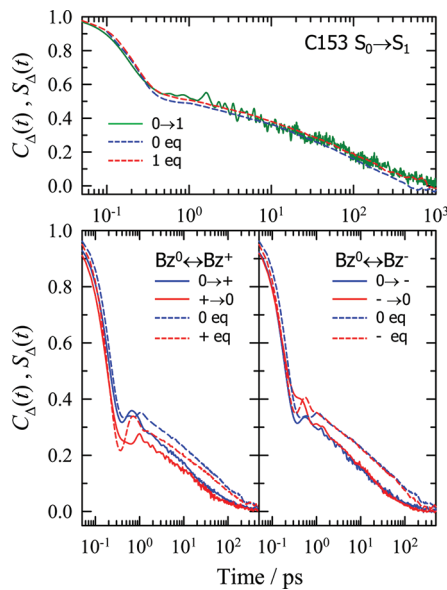


Figure 14. Comparison of nonequilibrium response functions ($S_{\Delta}(t)$, solid curves) and equilibrium time correlation functions ($C_{\Delta}(t)$, dashed curves) corresponding to the $S_0 \rightarrow S_1$ transition in C153 and charge perturbations in Bz.

find that $C_{\Delta}(t)$ calculated in the final solute state provides a slightly better representation of the nonequilibrium dynamics. In the present case, $S_{\Delta}(t)$ and the $C_{\Delta}^{(1)}(t)$ agree to within uncertainties. The situation is quite different for the Bz perturbations. Although the equilibrium $C_{\Delta}(t)$ functions of Bz^0 , Bz^+ , and Bz^- are all very similar (Figure 9), so that one might expect a linear response to be valid, the nonequilibrium $S_{\Delta}(t)$ functions are systematically faster than their $C_{\Delta}(t)$ counterparts, both in the initial Gaussian component and in the long-time response. Fits to eq 15 show that the slow solvation component is approximately three times faster in the $S_{\Delta}(t)$ response compared to the corresponding $C_{\Delta}(t)$ tcf.

The fact that the $S_{\Delta}(t)$ response functions decay much more rapidly than the $C_{\Delta}(t)$ correlation functions can be attributed to the local heating that results from the large amount of energy deposited into the solvent by the change of a full electronic charge in these solutes. The change in solute–solvent interaction energies in the $Bz^- \leftrightarrow Bz^0 \leftrightarrow Bz^+$ perturbations is ~430 kJ/mol (Table 2). Assuming that the system potential energy changes by one-half of this amount,⁸⁸ based on the heat capacity $C_v = 75 \text{ J K}^{-1} \text{ mol}^{-1}$ for ILM2⁶¹ the net temperature rise resulting from these perturbations is predicted (and observed at 1 ns) to be ~8 K. On the basis of the equilibrium data in Figure 11 such a change in temperature should produce only a 30% speed-up of the solvation response. However, the kinetic energy is not deposited uniformly in the system. At subpicosecond times this kinetic energy resides in translational motions of first solvation shell ions where it is equivalent to temperatures of hundreds of Kelvin above the bulk (see Figure S5, Supporting Information). Most of this kinetic energy flows into the surroundings within 10 ps, but its presence at earlier times is sufficient to decrease the time constant associated with the slow solvation component (τ_0) from ~35 ps in the equilibrium systems to ~11 ps in the nonequilibrium systems. The energy involved in the C153 transition is only about 10% of the energies in these charge perturbations, and it is initially deposited in a larger spatial region, which explains the applicability of the linear response approach. Given that the

C153 case is representative of the types of perturbations used to measure solvation dynamics experimentally it seems reasonable to expect linear response to apply to most experimental systems. This conclusion is supported by the results of Shim et al.,³⁰ who reported that perturbations of NP \leftrightarrow IP, which entail a much larger perturbation, also approximately conform to linear response predictions, at least at short times.

3.D. Solvation Mechanism. We finally consider what the simulations indicate about the “mechanism” of solvation in ionic liquids, employing the results from the nonequilibrium Bz charge perturbations just discussed. These simulations allow the simplest direct view of the relationship between changes in solvation structure and their energetic consequences. Despite the heating effect present in these simulations, we anticipate that the underlying mechanisms revealed will also describe dynamics in the linear regime.

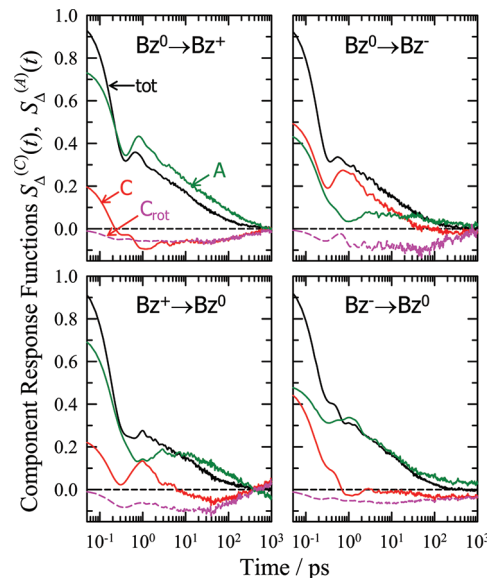


Figure 15. Nonequilibrium response functions ($S_{\Delta}(t)$, black curves) corresponding to four charge perturbations in Bz solutes and their decomposition into contributions from cations ($S_{\Delta}^C(t)$; solid red curves) and anions ($S_{\Delta}^A(t)$; green curves). Dashed pink curves labeled C_{rot} are the approximate contributions of cation rotations according to eq 19.

Figure 15 shows the solvation responses to the four Bz charge perturbations decomposed into cation (C) and anion (A) contributions defined by

$$S_{\Delta}(t) = S_{\Delta}^C(t) + S_{\Delta}^A(t) \quad (18a)$$

where

$$S_{\Delta}^X(t) = \frac{\langle \Delta U_{\text{EI}}^X(t) - \Delta U_{\text{EI}}^X(\infty) \rangle}{\langle \Delta U_{\text{EI}}(0) - \Delta U_{\text{EI}}(\infty) \rangle} \quad (X = C, A) \quad (18b)$$

The values of $S_{\Delta}^X(0)$ indicate the relative contributions of cation and anion motions to the overall response $\langle \Delta U_{\text{EI}}(0) - \Delta U_{\text{EI}}(\infty) \rangle$. The fact that all component contributions are positive at $t = 0$ means that net ion motions are in the directions expected. For example, if the solute charge becomes more positive (as in $Bz^0 \rightarrow Bz^+$ and $Bz^- \rightarrow Bz^0$) both types of

ions move to decrease the electrical potential at the solute charge site, i.e., anions move toward the solute and cations move away and/or rotate appropriately. Figure 15 also indicates that there is an asymmetry to the cation and anion contributions. When the solute charge is positive, the response is dominated by anion motions. In the case of the $\text{Bz}^0 \rightarrow \text{Bz}^+$ and $\text{Bz}^+ \rightarrow \text{Bz}^0$ perturbations 75–77% of the response is from the anions. However, the reverse is not found for negatively charged solutes. In the $\text{Bz}^0 \rightarrow \text{Bz}^-$ and $\text{Bz}^- \rightarrow \text{Bz}^0$ perturbations the cation and anion contributions are nearly equal, 47–50%. Such asymmetry has also been observed in previous simulations.^{30,38–40} At least in the present case it probably reflects the more localized character of the anion charge relative to that of the cation. Another interesting feature of the decompositions in Figure 15 is that the cation response $S_{\Delta}^C(t)$ is often negative at longer times, indicating an “over-response” by cations at early times, which is compensated by a contrary motion at longer times. Similar cation over-response can be seen in the decompositions of equilibrium tcfs corresponding to charge perturbations in Bz^0 and Bz^+ shown in Figure S6, Supporting Information (see also refs 38 and 40). Cation rotation appears to be the source of this behavior.

The dashed curves labeled “ C_{rot} ” in Figure 15 provide an indication of the effect of cation rotation on the solvation response. These curves were derived by first calculating the interaction energies that would result from all cation charge being located at the cation center of mass rather than being distributed among the three cation sites. The response functions $S_{\Delta}^{\text{com}}(t)$ so generated all lie parallel to but slightly above (by an average of 9%) the actual $S_{\Delta}^C(t)$ data at early times. On the basis of this parallelism, we assumed that when properly rescaled these center-of-mass functions approximate the translation contribution of cations. The rotational contribution is then approximated by the difference between $S_{\Delta}^C(t)$ and $S_{\Delta}^{\text{com}}(t)$

$$S_{\Delta}^{\text{trans}}(t) \cong \{S_{\Delta}^C(0)/S_{\Delta}^{\text{com}}(0)\}S_{\Delta}^{\text{com}}(t) \quad (19a)$$

$$S_{\Delta}^{\text{rot}}(t) \cong S_{\Delta}^C(t) - S_{\Delta}^{\text{trans}}(t) \quad (19b)$$

Three things are suggested by these rotational estimates. First, the magnitude of $S_{\Delta}^{\text{rot}}(t)$ remains less than 0.15 at all times, suggesting that rotation plays a relatively minor role in the overall solvation response. This observation is consistent with the prior simulation results of Shim and Kim³⁷ and Kobrak,^{38–40} who analyzed the short-time solvation dynamics in several model imidazolium ionic liquids.⁸⁹ Figure 15 shows that the rotational contribution becomes relatively more important at longer times, and in most cases the cation response is nearly all rotational at times greater than 100 ps. This temporal separation of rotational and translational contributions is similar to what has been found in simulations of the dielectric response of neat ionic liquids.^{90,34} Finally, the translational cation contribution (not shown) remains positive, whereas $S_{\Delta}^{\text{rot}}(t)$ is everywhere negative. This difference suggests an interpretation of the negative going regions of $S_{\Delta}^C(t)$ as being due to the slower rotational motions of cations adjusting for over polarization due to earlier translational motions.

Figure 16 exposes some of the details of the translational motions of solvent ions in the form of contour maps of the time-dependent radial distribution functions $g_{\text{com}}^X(r,t)$ of components $X = \text{C}, \text{A}$. The two perturbations $\text{Bz}^0 \leftrightarrow \text{Bz}^-$ are shown in Figure 16, and corresponding plots for the $\text{Bz}^0 \leftrightarrow \text{Bz}^+$ perturbations are provided as Figure S7, Supporting Informa-

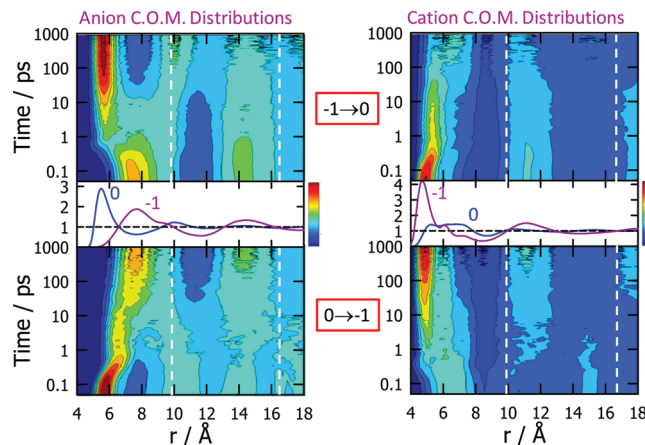


Figure 16. Contour plots of time-dependent center-of-mass radial distribution functions of solvent anions (left) and cations (right) in response to the charge perturbations $\text{Bz}^- \rightarrow \text{Bz}^0$ (top) and $\text{Bz}^0 \rightarrow \text{Bz}^-$ (bottom). Center panels show the equilibrium distributions of Bz^0 and Bz^- . White dashed reference lines indicate the locations of the first (9.8 Å) and second (16.3 Å) complete (+/-) charge shells of the Bz^- solute as defined by the $v(r)$ data in Figure 5.

tion. For reference, the dashed lines in Figure 16 locate the first (9.8 Å) and second (16.3 Å) “complete” solvation shells, i.e., charge shell regions (1 + 2) and (3 + 4) in Figure 5. We will describe the features of $g_{\text{com}}^X(r,t)$ for the $\text{Bz}^- \rightarrow \text{Bz}^0$ perturbation (bottom panels in Figure 16) in some detail as they illustrate the general features found in all four of these cases. Prior to the perturbation there is a relatively well-ordered shell of anions approximately in contact with the Bz^0 solute. Cations are also in contact with the Bz^0 solute, but the polyatomic structure of the cations renders $g_{\text{com}}^{\text{C}}(r,0)$ broad and featureless in this region. When the solute is suddenly charged, nearest-neighbor anions feel a strong instantaneous repulsion and cations an instantaneous attraction to the solute. Inertia-limited motion of these anions to larger distances is signaled by the rapid decrease in the height of the peak of $g_{\text{com}}^{\text{A}}$ and a small shift from 5.8 to 6.5 Å within the first 600 fs. A comparable influx of cations also occurs during this period, but the breadth of $g_{\text{com}}^{\text{C}}$ makes it difficult to discern the change in Figure 16. We also note that the oscillation seen in $S_{\Delta}^C(t)$ in Figure 15 during this time period reflects a slight rebound in the peak of $g_{\text{com}}^{\text{C}}(r,t)$ which is not noticeable here. Clearer examples of such rebounds are found in the $g_{\text{com}}^{\text{A}}(r,t)$ distributions in Figure S7, Supporting Information. When the inertial phase of the motion ends in about 1 ps, roughly 70% of the total change in solvation energy has occurred. At this point the solvation structure characteristic of the neutral Bz^0 solute has been destroyed, but the features of the distribution functions are still far removed from those of the charged solute Bz^- . The final structure appears to build up continuously over times between one and several hundred picoseconds. For example, the peak of $g_{\text{com}}^{\text{A}}$ only shifts from an intermediate location of 6.5 Å to nearer to its final location at 7.6 Å after ~30 ps. Minima and maxima in regions beyond the first complete solvation shell ($r > 9.8$ Å) only achieve their final values at times of ~500 ps when relaxation of the solvation energy is >95% complete.

Scenarios comparable to this one for $\text{Bz}^0 \rightarrow \text{Bz}^-$ describe the action in the three other Bz charge perturbations. In all cases the sudden imbalance of electrical forces leads to impulsive motion of ions into and/or out of the first solvation shell. These motions result in large changes to the structure of the

first solvation shell within the first picosecond after the perturbation is applied. Oscillations in $S_{\Delta}(t)$ within this initial period reflect first solvation shell ions rebounding from the solute or from second-shell neighbors. However, although much structural change and energy relaxation occurs within the first 1 ps, the finer features in g_{com}^X and the ultimate energy characteristic of the final solute state are attained much more slowly, over periods of tens to hundreds of picoseconds.

Whereas the 2d representations shown in Figure 16 provide a global view of the dynamics, 1d representations (Figure 17)

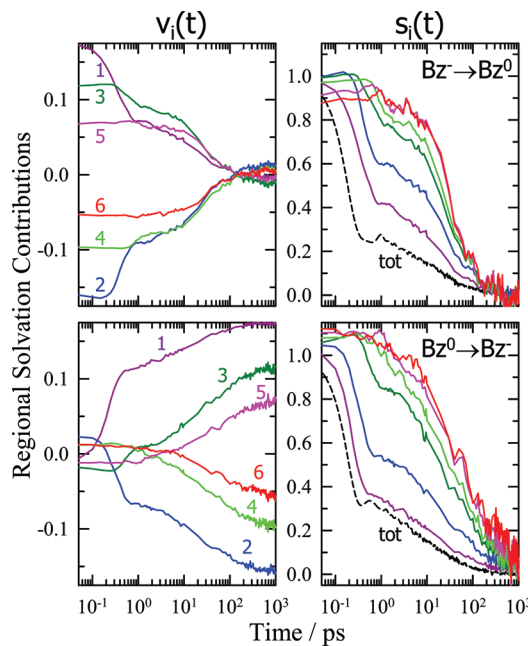


Figure 17. Spatial decomposition of the solvation response to the charge perturbations $\text{Bz}^- \rightarrow \text{Bz}^0$ (top) and $\text{Bz}^0 \rightarrow \text{Bz}^-$ (bottom). (Left) Contributions to the electrical potential at the solute center from regions 1–6 defined in Figure 5. Outer radii are 6.05, 9.8, 12.8, 16.3, 19.5, and 22.9 Å. (Right) Normalized regional response functions $s_i(t) = \{v_i(t) - v_i(\infty)\}/\{v_i(0) - v_i(\infty)\}$ and the total solvation response $S_{\Delta}(t)$ (dashed curves).

make it easier to relate the time-dependent structural changes taking place to the solvation energy response. Rather than examining features of g_{com}^X for this purpose, we instead employ the reaction potential contributions introduced in eq 8. The left-hand panels of Figure 17 show time-dependent reaction

potential contributions, $v(r,t)$, in $\text{Bz}^0 \leftrightarrow \text{Bz}^-$ charge perturbations integrated over the spatial regions 1–6 defined by the equilibrium $v(r)$ shown in Figure 5. Corresponding plots of $\text{Bz}^0 \leftrightarrow \text{Bz}^+$ data are provided in Figure S8, Supporting Information. Summing over these regional contributions, $v_i(t)$, provides the net electrical potential at the solute charge site $\langle V(t) \rangle = \sum_i \langle v_i(t) \rangle$, which for these solutes is directly proportional to $\langle \Delta U_{\text{El}}(t) \rangle$. Thus, the $v_i(t)$ provide a spatial decomposition of the solvation response $S_{\Delta}(t)$. To compare dynamics in different regions, we calculate the normalized response function for each region

$$s_i(t) = \frac{\langle v_i(t) \rangle - \langle v_i(\infty) \rangle}{\langle v_i(0) \rangle - \langle v_i(\infty) \rangle} \quad (20)$$

and these functions are shown in the right-hand panels of Figure 17 together with $S_{\Delta}(t)$. In all cases one finds that the time dependence of region 1 ($r < 6 \text{ \AA}$) most closely resembles that of the total solvation response. With the exception of the $\text{Bz}^- \rightarrow \text{Bz}^0$ perturbation, where the difference is larger, $s_1(t)$ is uniformly slower than $S_{\Delta}(t)$ by roughly a factor of 2. At larger distances from the solute the regional response functions extend to progressively longer times. Subpicosecond dynamics are only prominent in regions 1 and 2 ($r < 10 \text{ \AA}$). Beyond region 4 ($r > 19 \text{ \AA}$) no subpicosecond component appears to be present. (As will be shown later, there is some subpicosecond motion in all regions but its effect is too small to observe here.) The picture suggested by this analysis is that the strong electrostatic forces in the immediate vicinity of the solute first cause an inertial restructuring of nearby ions. This local disturbance then propagates outward to induce the more subtle restructuring of solvation shells farther away from the solute.

Such a description, while pleasing, should be viewed with some caution. As already discussed in section 3.A, the long-range coupling among solvent ions necessarily makes spatial decompositions of solvation energies ambiguous.⁹¹ One can appreciate this fact from Figure 17 itself, where one can view the regional $v(t)$ responses to occur in pairs (1,2), (3,4), and (5,6). The members of each of these pairs display similar dynamics but have nearly equal and oppositely signed magnitudes, which leads to considerable cancellation upon summation. In the same way that assigning fractional contributions to the solvation energy via the artifice of using the unsigned areas in Figure 5 is only suggestive, so too is the

Table 5. Properties Associated with Bz Solvation and with $\text{Bz}^0 \rightarrow \text{Bz}^{\pm}$ Differences^a

no.	$R_{\text{in}} - R_{\text{out}}/\text{\AA}$	$ \langle v_i \rangle /\langle V \rangle $	Bz^+			Bz^0			Bz^-			$\text{Bz}^0 \rightarrow \text{Bz}^+$			$\text{Bz}^0 \rightarrow \text{Bz}^-$			
			N_{av}	N_C	N_A	$\langle v_i \rangle/\text{au}$	N_{C}	N_A	$\langle v_i \rangle/\text{au}$	N_C	N_A	$\langle v_i \rangle/\text{au}$	ΔN_C	ΔN_A	$\delta r/\text{\AA}$	ΔN_C	ΔN_A	$\delta r/\text{\AA}$
1	3.0–6.1	0.61	5.6	0.6	6.2	-0.20	2.3	3.1	-0.005	4.4	0.3	0.18	-1.6	+3.1	1.4	+2.1	-2.8	2.4
2	6.1–9.8	0.39	17	12	3.9	0.20	8.9	8.0	0.014	5.5	12	-0.16	+2.8	-4.2	1.8	-3.4	+4.2	1.5
3	9.8–12.8	0.27	27	11	17	-0.14	14	13	-0.011	17	9	0.12	-3.0	+4.1	1.4	+3.6	-4.3	1.5
4	12.8–16.3	0.21	53	30	22	0.10	27	26	0.004	23	31	-0.10	+3.2	-4.3	1.0	-3.7	+4.5	1.0
5	16.3–19.6	0.17	76	34	42	-0.08	38	38	-0.004	41	34	0.07	-3.3	+3.9	0.7	+3.3	-4.1	0.8
6	19.6–22.9	0.14	106	57	49	0.06	54	53	0.004	50	57	-0.06	+2.9	-3.6	0.6	-3.4	+4.0	0.7

^a R_{in} and R_{out} define the regions examined (approximately the zero crossings of $v(r)$ of Bz^{\pm}). $|v_i/\langle V \rangle|$ is the magnitude of the ratio of the electrical potential at the solute center produced by an ion at an average distance within a given region to the net electrical potential of Bz^{\pm} solutes (0.13 au). N_{av} is the number of ions in a given region averaged over the three Bz solutes. N_C , N_A , and $\langle v_i \rangle$ are the numbers of cations and anions and the average electrical potential contribution in equilibrium with the three Bz solutes. ΔN_C and ΔN_A are changes in cation and anion numbers, and δr is an effective average displacement of ions (eq 21; see text) associated with the $\text{Bz}^0 \rightarrow \text{Bz}^{\pm}$ perturbations.

variation in the individual response times of these differently signed regions.

The last aspect of the solvation “mechanism” we consider is the amount by which individual ions move during the solvation response. Tables 5 and 6 provide some data pertinent to this

Table 6. Radial Displacements in $Bz^0 \rightarrow Bz^-$ and Bz^0 Simulations^a

t/ps	$Bz^0 \rightarrow Bz^-$			Bz^0		
	$S_\Delta(t)$	$\Delta r_C^{\text{rms}}/\text{\AA}$	$\Delta r_A^{\text{rms}}/\text{\AA}$	$C_\Delta(t)$	$\Delta r_C^{\text{rms}}/\text{\AA}$	$\Delta r_A^{\text{rms}}/\text{\AA}$
0.10	0.79	0.2	0.1	0.80	0.1	0.1
0.20	0.50	0.3	0.2	0.48	0.3	0.3
1	0.30	0.7	0.7	0.35	0.6	0.6
10	0.15	1.0	1.0	0.23	0.8	0.8
100	0.03	1.7	1.4	0.09	1.4	1.4
1000	<0.01	4.9	4.7	<0.01	3.5	3.2

^aRoot mean squared displacements are defined by $\Delta r_X^{\text{rms}} = (\langle (\Delta r_X(t)^2) \rangle)^{1/2}$ where averaging is performed over all ions of a given type ($X = C, A$). In the nonequilibrium $Bz^0 \rightarrow Bz^-$ case $\Delta r_X(t)$ denotes radial displacement of an ion at time t after the solute perturbation observed in the single trajectory depicted in Figure 18. In the Bz^0 case, values are from long equilibrium simulations and therefore averaged to a much greater degree.

question. Table 5 summarizes quantities associated with solvation of Bz solutes in equilibrium and with the net changes involved in $Bz^0 \rightarrow Bz^\pm$ perturbations, again partitioned according to the charge regions of Figure 5. An indication of the collective nature of the solvation response is provided in the column labeled $|v_1/\langle V \rangle|$ in Table 5. Listed here are the magnitudes of the average electrical potentials at the center of Bz^\pm solutes produced by a single ion within a given region ($|v_1(i)|$) divided by the net electrical potential ($\langle V \rangle = \mp 0.13$ au). The column labeled N_{av} contains the numbers of ions (averaged over all three Bz solutes) in each region. From these data one sees that each of the 5–6 ions within the first charge shell is capable of providing over 60% of the net electrical potential or net solvation energy ($\langle U_{\text{el}} \rangle$) of a Bz^\pm solute. If one sums unsigned interactions of the solute with the 285 ions contained within the first 6 charge shells, one finds that the available Coulomb energy is roughly 60 times $\langle U_{\text{el}} \rangle$. These observations underscore the fact that solvation in ionic liquids entails a delicate balance between a large number of strong interactions, i.e., is a highly collective phenomenon.³⁸

Two measures of the extent of ion motion required to account for the net solvation differences between Bz^0 and Bz^\pm are provided by the columns ΔN_C , ΔN_A , and δr in Table 5. $\Delta N_{C,A}(i)$ are the changes in cation and anion numbers within region i between the initial and final equilibrium states. As shown by the $\Delta N_{C,A}(i)$ data, the structural change required after charging a neutral Bz^0 solute consists of exchanging roughly 3–4 cations for anions in each region. Given the alternating surfeits and deficits of ions of a given type in successive charge shells, it seems reasonable to view the motions responsible for the structural change to entail C–A exchanges of a few ions over distances of roughly one-half of a shell thickness, ~ 1.7 Å. Such a displacement is about 30% of an average ion diameter (5.8 Å). An alternative perspective on the motion required is provided by the values of $\delta r(i)$, defined by

$$\delta r(i) = \left| \frac{\bar{r}_i^2 \langle \Delta v_i \rangle}{q[N_A(i) + N_C(i)]} \right| \quad (21)$$

In this expression \bar{r}_i is the average radius of region i , $\langle \Delta v_i \rangle = \langle v_i(0) \rangle - \langle v_i(\infty) \rangle$, and $q = 0.78e$ is the magnitude of the solvent ion charge. These $\delta r(i)$ are the average radial displacements required to effect the net change in regional potential contributions v_i , assuming that all ions move in the appropriate directions. These estimates are also on the order of 1–2 Å.

Finally, a view of what individual ions are doing in response to a $Bz^0 \rightarrow Bz^-$ perturbation is provided in Figure 18. Shown

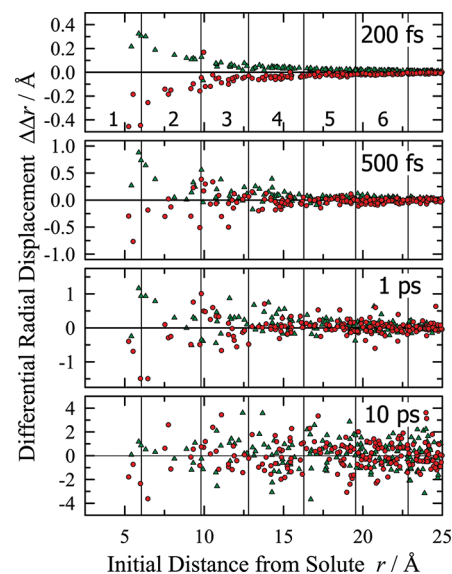


Figure 18. Differential radial displacements $\Delta\Delta r(t)$ of cations (red circles) and anions (green triangles) observed at selected times during a single trajectory of a $Bz^0 \rightarrow Bz^-$ charge perturbation. $\Delta\Delta r(t)$ is defined by $\Delta\Delta r(t) = \{r(t) - r(0)\}_{0 \rightarrow t}^{\text{ne}} - \{r(t) - r(0)\}_0^{\text{eq}}$, where “ne” refers to a simulation where the charge perturbation is applied at $t = 0$ and “eq” to a simulation in which no perturbation is applied. Locations of charge shells 1–6 are indicated by the vertical lines in each panel.

here are differences in the radial displacements ($\Delta r = r(t) - r(0)$) between a single trajectory in which the $Bz^0 \rightarrow Bz^-$ perturbation is applied at $t = 0$ and a control trajectory in which the Bz^0 solute is unperturbed. When the perturbation is applied, solvent ions feel an instantaneous impulsive force whose magnitude dies off as r^{-2} . This force initiates an inertial motion of ions which lasts for between 200 and 400 fs (top panel of Figure 18) until they collide with one or more neighboring ions and memory of initial velocities is lost. The perturbed motion of ions nearest the solute (regions 1 and 2) amounts to less than 1 Å during this inertial period. The ions in more distant regions alter their trajectories to a much lesser extent (~ 0.1 Å) as a result of the perturbation. Note, however, even in region 6 there has been some change in ion motions in direct response to the solute perturbation. After this brief inertial regime, the motion of ions takes on a diffusive character and is such that after about 1 ps the differences between the perturbed and the unperturbed trajectories become too subtle to discern. In this diffusive regime the chaotic motions of ions are much larger than their response to the now small residual force created by the perturbation.

The extent of motion during this diffusive regime is quantified in Table 6, which lists system-averaged root-mean square radial displacements of cations and anions measured in the perturbed trajectory. The average diffusive displacements of

ions over the period 10–100 ps are of the same extent we just showed was sufficient to relax structural and energetic differences between equilibrium solvation of Bz^0 and Bz^- , i.e., 1–2 Å. As shown by the column labeled $S_\Delta(t)$ in Table 6, nearly all of the solvation response is complete over such times. Also listed in Table 6 are values of $C_\Delta(t)$ and the root-mean-squared displacements observed in a system in equilibrium with the Bz^0 solute. As already discussed, $S_\Delta(t)$ decays more quickly than $C_\Delta(t)$ due to local heating, and for this same reason ion displacements are also slightly larger for the nonequilibrium system than the equilibrium one. Nevertheless, the observations concerning the extent of ion motion are much the same in the nonequilibrium and equilibrium cases. We conclude that in both the inertial and the diffusive regimes solvation is effected by individual ions making excursions that amount to only about 20–30% of their diameters. The relative importance of inertial versus diffusive motions varies with initial position relative to the solute. Nearby ions move the required amount primarily through inertial motions in direct response to the initial impulsive perturbation, whereas ions far from the solute respond almost entirely through random diffusive motions only very subtly biased by the solute perturbation.

4. SUMMARY AND CONCLUSIONS

We used simulations of a variety of solutes in a coarse-grained model of an ionic liquid in order to examine some of the fundamental features of ionic liquid solvation. Although a number of simulations of this sort have already been performed,^{28–52} use of this simplified solvent model, together with equally simple immobile solutes, has afforded a much better look at the long time dynamics and provided new insights into mechanistic aspects of solvation in ionic liquids.

Comparisons of the structure and the energetics of solvation in ILM2 and the prototypical high-polarity dipolar solvent CH_3CN reveal both similarities and differences. The charge ordering in the presence of ionic solutes is qualitatively similar in the two solvents, but the range of the interaction differs significantly (Figure 5). Although rigorous decomposition of electrostatic energies into spatial regions is not possible, a schematic analysis shows that whereas ~60% of the electrostatic solvation energy of a benzene-size solute comes from the first complete charge shell (16 solvent molecules) in CH_3CN , this same fraction of the solvation energy is only achieved in three complete charge shells in ILM2, a region which encompasses more than 10 times this number of solvent ions.

Despite this difference in solvation range, solvation energies in the two solvents are remarkably similar (Figure 6). In nearly all of the solutes examined here electrostatic solute–solvent interaction energies in ILM2 are within 10% of those in CH_3CN . This correspondence between solvation energies in ionic liquids and high-polarity dipolar solvents is consistent with what has previously been found in numerous solvatochromic^{19,78,10} and other⁹² experiments.

Electrostatic solute–solvent interaction energies, $\langle U_{\text{El}} \rangle$, of spherical monatomic ions in ILM2 and its size-scaled variants can be represented with good accuracy in terms of solute (R_u) and average solvent ion radii (R_v) by $\langle U_{\text{El}} \rangle \approx -q^2/(aR_u + bR_v)$ with $a = 0.86$ and $b = 0.40$ (Figure 7). This correlation should be of use for making first estimates of ion solvation energies in real experimental systems.

Solvation energies associated with changes of $\pm 1e$ follow linear response predictions to a moderate degree. Fluctuations in electrostatic energy differences ($\delta\Delta U_{\text{El}}$) are Gaussian up to

$>10 k_{\text{B}}T$; however, linear response predictions of energy changes corresponding to such perturbations are typically only accurate to about 25% in the systems studied.

Solvation time correlation functions in ILM2 and CH_3CN (Figure 8) show a qualitatively similar biphasic character. In both solvents $C_\Delta(t)$ consists of a subpicosecond inertial component and a longer component due to diffusive solvent motions. The obvious difference between the two solvents is the fact that the diffusive component is on the order of 100-fold slower and temporally much more disperse in the ionic liquid. Systematic trends are found in both the fast and the slow components of solvation as a function of solute size (Figure 10a). The effects are much larger in correlation functions associated with dipolar solute perturbations compared to charge perturbations.

As a function of temperature, correlation times in ILM2 are found to be proportional to viscosity (η/T), similar to what has been observed experimentally (Figure 11).^{83,7,18,17} Comparison of simulated and experimental dynamics associated with the $S_0 \rightarrow S_1$ transition in coumarin 153 (C153; Figure 12) indicates that the simulations exhibit the same basic time scale and character of the fast and slow components found in experiment, but the amplitude of the fast component is exaggerated. Jeong et al.³¹ have shown that solute polarizability tends to decrease the amplitude of the fast solvation component, and it seems likely that incorporation of explicit solute and solvent⁹³ polarizability into the simulation model would provide closer agreement with experiment. Nevertheless, the level of agreement with the idealized models employed here is sufficiently good that one can have some confidence that the present results are of direct relevance to experimental measurements of solvation dynamics.

Solute motion is found to have a significant influence on solvation times, even in the case of relatively large solutes (Figure 13). For example, in C153 the slow component of solvation is nearly 2-fold faster when the solute is allowed to rotate and translate compared to when it is held immobile. Much larger effects are found for small solutes like the neutral diatomic (NP) studied by Shim and Kim^{28–30} due to fact that such solutes undergo relatively rapid large-angle rotational jumps in ionic liquids.⁵⁶ Solute motion has typically been ignored in experimental studies of solvation dynamics in conventional dipolar solvents, where it has generally been assumed to be of relatively minor importance. The applicability of dielectric continuum models of solvation tends to support this assumption in dipolar solvents.⁹⁴ However, the situation appears to be different in ionic liquids, perhaps because of the generally larger size of ionic liquid molecules and/or the relatively greater importance of translational motions in ionic solvation. Additional simulations focused on solute motional effects and the relative importance of rotational versus translational solute motions will be needed to aid in the proper interpretation of experiments.

The applicability of linear response estimates of solvation dynamics was tested for two limiting sorts of perturbations: the $S_0 \rightarrow S_1$ transition in C153 and changes of a full electronic charge in benzene-size solutes ($\text{Bz}^0 \leftrightarrow \text{Bz}^\pm$; Figure 14). Whereas linear response estimates are accurate in the former case, the nonequilibrium responses to the Bz charge perturbations are 3-fold faster due to local heating. Given the amount of energy deposited in the latter case, observation of a heating effect is not surprising. It is therefore interesting to recall that early studies of solvation in acetonitrile⁸⁷ also

monitored local heating in similar charge perturbations (see Figure 13 of ref 87) and yet reported good agreement between nonequilibrium and equilibrium simulations. A number of factors could be responsible for this difference. The fact that the diffusive dynamics are much more temperature sensitive in ionic liquids than they are in a nonassociated solvent like acetonitrile is likely to be the largest contributor. (For example, the viscosity activation energy in $[\text{Im}_{41}][\text{PF}_6]^{95}$ is nearly 6 times larger than in CH_3CN .⁹⁶) Further study of such differences would be interesting, but it should be noted that in experimental systems or more realistic solvent models the effects will be muted by the presence of low-frequency internal modes which can accept some portion of the solvation energy released.

Simulations of $\text{Bz}^0 \leftrightarrow \text{Bz}^\pm$ perturbations revealed several general features of the solvation “mechanism” in ILM2. Anion motions are relatively more important than cation motions in effecting changes in solvation energy, especially during the inertial portion of the response (Figure 15). This asymmetry is due to the greater charge concentration in the anion of ILM2. Similar findings in previous studies^{30,38–40} suggest that this relatively greater importance of anion motions is likely to hold true in ionic liquids containing anions such as Cl^- , BF_4^- , and PF_6^- .

Translational motions were found to be much more important in the solvation response compared to rotational motions. During the inertial phase of the dynamics ion rotation play a negligible role. At longer times cation rotations appear to adjust for excess polarization produced by anion and cation translations. Given the small dipole moment (3.0 D) of the cation of ILM2, this modest role of rotational motion is expected.⁹⁷ Although rotational motions could play a more important role in other liquids, it seems most useful to view charge solvation in ionic liquids as resulting primarily from ion translation and to relegate ion rotations to the status of a second-order effect. Such a description is just the opposite to the situation pertaining in a dipolar solvent like CH_3CN where charge solvation is driven predominantly by solvent molecule rotations and solvent translation has little impact.⁸¹ However, it should be noted that these conclusions made on the basis of charge perturbations in atomic solutes will be modified in the case of polyatomic solutes having more complex charge redistributions. For the same reason that solvent molecule translation becomes progressively more important in solvation by CH_3CN when the multipole order of the perturbation increases,⁸¹ rotational motions might be expected to play a larger role in solvation of more complex species and perturbations.

The mechanistic picture that emerges from this work is that the subpicosecond component of solvation is dominated by inertial translations of nearest-neighbor ions. Such motions are sufficient to relax a large fraction of the solvation energy. At times greater than 1 ps motions are diffusive in nature. At least schematically, the relative weight of diffusive versus inertial ion motions increases with distance from the solute as does the response time (Figure 17). Both near to and far from the solute rather little solvent motion is required (Figures 16 and 18). Successive charge shells in ILM2 are separated by ~ 3.3 Å, slightly more than one-half of an average ion diameter (Figure 5). Solvation requires redistribution of oppositely charged ions over distances of one-half of this separation, 1–2 Å, or roughly 30% of an average ion diameter.

ASSOCIATED CONTENT

S Supporting Information

This material is available free of charge via the Internet at <http://pubs.acs.org>.

AUTHOR INFORMATION

Corresponding Author

*E-mail: Maroncelli@psu.edu.

Present Address

[†]Department of Chemistry, New York University, New York, New York 10003, United States.

Notes

The authors declare no competing financial interest.

ACKNOWLEDGMENTS

This work was supported by the Division of Chemical Sciences, Geosciences, and Biosciences, Office of Basic Energy Sciences of the U.S. Department of Energy through grants DE-FG02-89ER14020 and DE-FG02-09ER16118. The authors thank Nikhil Patel for the initial work he did on this problem.

REFERENCES

- (1) Hallett, J. P.; Welton, T. *Chem. Rev.* **2011**, *111*, 3508.
- (2) In *Ionic Liquids in Synthesis*, 2nd ed.; Wasserscheid, P., Welton, T., Eds.; 2008.
- (3) Sun, P.; Armstrong, D. W. *Anal. Chim. Acta* **2010**, *661*, 1.
- (4) Armand, M.; Endres, F.; MacFarlane, D. R.; Ohno, H.; Scrosati, B. *Nat. Mater.* **2009**, *8*, 621.
- (5) Wishart, J. F. *Energy Environ. Sci.* **2009**, *2*, 956.
- (6) Samanta, A. J. *Phys. Chem. Lett.* **2010**, *1*, 1557.
- (7) Samanta, A. J. *Phys. Chem. B* **2006**, *110*, 13704.
- (8) Maroncelli, M.; Zhang, X.-X.; Liang, M.; Roy, D.; Ernsting, N. P. *Faraday Discuss. Chem. Soc.* **2012**, *154*, 409.
- (9) Arzhantsev, S.; Jin, H.; Baker, G. A.; Maroncelli, M. *J. Phys. Chem. B* **2007**, *111*, 4978.
- (10) Jin, H.; Baker, G. A.; Arzhantsev, S.; Dong, J.; Maroncelli, M. *J. Phys. Chem. B* **2007**, *111*, 7291.
- (11) Funston, A. M.; Fadeeva, T. A.; Wishart, J. F.; Castner, E. W. *J. Phys. Chem. B* **2007**, *111*, 4963.
- (12) Carlson, P. J.; Bose, S.; Armstrong, D. W.; Hawkins, T.; Gordon, M. S.; Petrich, J. W. *J. Phys. Chem. B* **2011**.
- (13) Chakrabarty, D.; Hazra, P.; Chakraborty, A.; Seth, D.; Sarkar, N. *Chem. Phys. Lett.* **2003**, *381*, 697.
- (14) Castner, E. W., Jr.; Margulis, C. J.; Maroncelli, M.; Wishart James, F. *Annu. Rev. Phys. Chem.* **2011**, *62*, 85.
- (15) Li, X.; Liang, M.; Chakraborty, A.; Kondo, M.; Maroncelli, M. *J. Phys. Chem. B* **2011**, *115*, 6592.
- (16) Liang, M.; Kaintz, A.; Baker, G. A.; Maroncelli, M. *J. Phys. Chem. B* **2012**, *116*, 1370.
- (17) Kimura, Y.; Fukuda, M.; Suda, K.; Terazima, M. *J. Phys. Chem. B* **2010**, *114*, 11847.
- (18) Nagasawa, Y.; Oishi, A.; Itoh, T.; Yasuda, M.; Muramatsu, M.; Ishibashi, Y.; Ito, S.; Miyasaka, H. *J. Phys. Chem. C* **2009**, *113*, 11868.
- (19) Poole, C. F. *J. Chromatogr. A* **2004**, *1037*, 49.
- (20) Lang, B.; Angulo, G.; Vauthhey, E. *J. Phys. Chem. A* **2006**, *110*, 7028.
- (21) Muramatsu, M.; Nagasawa, Y.; Miyasaka, H. *J. Phys. Chem. A* **2011**, *115*, 3886.
- (22) Jin, H.; Li, X.; Maroncelli, M. *J. Phys. Chem. B* **2007**, *111*, 13473.
- (23) Jin, H.; Li, X.; Maroncelli, M. *J. Phys. Chem. B* **2010**, *114*, 11370.
- (24) Santhosh, K.; Banerjee, S.; Rangaraj, N.; Samanta, A. *J. Phys. Chem. B* **2010**, *114*, 1967.
- (25) Sahu, K.; Kern, S. J.; Berg, M. A. *J. Phys. Chem. A* **2011**, *115*, 7984.
- (26) Hanke, C. G.; Price, S. L.; Lynden-Bell, R. M. *Mol. Phys.* **2001**, *99*, 801.

- (27) Maginn, E. J. *Rev. Comput. Chem.* **2009**, *26*, 421.
- (28) Shim, Y.; Duan, J.; Choi, M. Y.; Kim, H. J. *J. Chem. Phys.* **2003**, *119*, 6411.
- (29) Shim, Y.; Choi, M. Y.; Kim, H. J. *J. Chem. Phys.* **2005**, *122*, 044510.
- (30) Shim, Y.; Choi, M. Y.; Kim, H. J. *J. Chem. Phys.* **2005**, *122*, 044511.
- (31) Jeong, D.; Shim, Y.; Choi, M. Y.; Kim, H. J. *J. Phys. Chem. B* **2007**, *111*, 4920.
- (32) Shim, Y.; Kim, H. J. *J. Phys. Chem. B* **2007**, *111*, 4510.
- (33) Shim, Y.; Kim, H. J. *J. Phys. Chem. B* **2009**, *113*, 12964.
- (34) Shim, Y.; Kim, H. J. *J. Phys. Chem. B* **2008**, *112*, 11028.
- (35) Shim, Y.; Kim, H. J. *J. Phys. Chem. B* **2010**, *114*, 10160.
- (36) Znamenskiy, V.; Kobrač, M. N. *J. Phys. Chem. B* **2004**, *108*, 1072.
- (37) Kobrač, M. N.; Znamenskiy, V. *Chem. Phys. Lett.* **2004**, *395*, 127.
- (38) Kobrač, M. N. *J. Chem. Phys.* **2006**, *125*, 64502.
- (39) Kobrač, M. N. *J. Chem. Phys.* **2007**, *127*, 099903.
- (40) Kobrač, M. N. *J. Chem. Phys.* **2007**, *127*, 184507.
- (41) Margulis, C. J. *Mol. Phys.* **2004**, *102*, 829.
- (42) Hu, Z.; Margulis, C. J. *J. Phys. Chem. B* **2006**, *110*, 11025.
- (43) Hu, Z.; Margulis, C. J. *Proc. Natl. Acad. Sci.* **2006**, *103*, 831.
- (44) Annapureddy, H. V. R.; Hu, Z.; Xia, J.; Margulis, C. J. *J. Phys. Chem. B* **2008**, *112*, 1770.
- (45) Annapureddy, H. V. R.; Margulis, C. J. *J. Phys. Chem. B* **2009**, *113*, 12005.
- (46) Bhargava, B. L.; Balasubramanian, S. *J. Chem. Phys.* **2005**, *123*, 144505.
- (47) Lynden-Bell, R. M. *J. Phys. Chem. B* **2007**, *111*, 10800.
- (48) Pinilla, C.; DelPopolo, M. G.; Kohanoff, J.; Lynden-Bell, R. M. *J. Phys. Chem. B* **2007**, *111*, 4877.
- (49) Lynden-Bell, R. M. *J. Chem. Phys.* **2008**, *129*, 204503/1.
- (50) Streeter, I.; Lynden-Bell, R. M.; Compton, R. G. *J. Phys. Chem. C* **2008**, *112*, 14538.
- (51) Lynden-Bell, R. M. *Phys. Chem. Chem. Phys.* **2010**, *12*, 1733.
- (52) Song, X. *J. Chem. Phys.* **2009**, *131*, 044503.
- (53) Arzhantsev, S.; Jin, H.; Ito, N.; Maroncelli, M. *Chem. Phys. Lett.* **2006**, *417*, 524.
- (54) Jeong, D.; Choi, M. Y.; Jung, Y.; Kim, H. J. *J. Chem. Phys.* **2008**, *128*, 174504.
- (55) Grote, R. F.; Hynes, J. T. *J. Chem. Phys.* **1980**, *73*, 2715.
- (56) Shim, Y.; Jeong, D.; Choi, M. Y.; Kim, H. J. *J. Chem. Phys.* **2006**, *125*, 061102.
- (57) Shim, Y.; Kim, H. J. *J. Chem. Phys.* **2006**, *125*, 024507.
- (58) Mandal, P. K.; Paul, A.; Samanta, A. *J. Photochem. Photobiol. A* **2006**, *182*, 113.
- (59) Maroncelli, M.; Fleming, G. R. *J. Chem. Phys.* **1987**, *86*, 6221.
- (60) Roy, D.; Patel, N.; Conte, S.; Maroncelli, M. *J. Phys. Chem. B* **2010**, *114*, 8410.
- (61) Roy, D.; Maroncelli, M. *J. Phys. Chem. B* **2010**, *114*, 12629.
- (62) Merlet, C. I.; Salanne, M.; Rotenberg, B.; Madden, P. A. *J. Phys. Chem. C* **2011**, *115*, 16613.
- (63) Edwards, D. M. F.; Madden, P. A.; McDonald, I. R. *Mol. Phys.* **1984**, *51*, 1141.
- (64) Li, H.; Arzhantsev, S.; Maroncelli, M. *J. Phys. Chem. B* **2007**, *111*, 3208.
- (65) In *DL_POLY_2.13*; Smith, W., Forester, T. R., Eds.; CCLRC Daresbury Laboratory: Daresbury, UK, 2001.
- (66) Adams, D. J.; Dubey, G. S. *J. Comput. Phys.* **1987**, *72*, 156.
- (67) This relation here would be an equality apart from the fact that the nonequilibrium simulations are run at constant energy and a small amount of heating accompanies the solute perturbation.
- (68) Maroncelli, M.; Fleming, G. R. *J. Chem. Phys.* **1988**, *89*, 5044.
- (69) Carter, A. E.; Hynes, J. T. *J. Chem. Phys.* **1991**, *94*, 5961.
- (70) Laird, B. B.; Thompson, W. H. *J. Chem. Phys.* **2007**, *126*, 211104.
- (71) Hummer, G.; Pratt, L. R.; García, A. E. *J. Phys. Chem.* **1996**, *100*, 1206.
- (72) Hummer, G.; Pratt, L. R.; Garcia, A. E. *J. Chem. Phys.* **1997**, *107*, 9275.
- (73) Figueirido, F.; Del Buono, G. S.; Levy, R. M. *J. Phys. Chem. B* **1997**, *101*, 5622.
- (74) Lynden-Bell, R. M.; Rasiash, J. C. *J. Chem. Phys.* **1997**, *107*, 1981.
- (75) We note that eq 5 differs by a factor of 1/2 compared to the equations in ref 72 due to the fact that the latter apply to solvation free energies whereas we discuss electrostatic interaction energies.
- (76) These functions can be compared to the charge distribution functions $Q(r)$ ⁷⁷ used to describe charge ordering in the neat ionic liquid.^{61,60} $v(r) \cong 4\pi r Q(r)$ except that the $Q(r)$ were calculated from $g_{com}(r)$ assuming charges to be located on ion centers of mass, whereas $v(r)$ is calculated from the true distribution of charges among solvent sites. The difference is small in the present case.
- (77) Kebinski, P.; Eggebrecht, J.; Wolf, D.; Phillipot, S. R. *J. Chem. Phys.* **2000**, *113*, 282.
- (78) Reichardt, C. *Green Chem.* **2005**, *7*, 339.
- (79) Lynden-Bell, R. M. *Electrochim. Commun.* **2007**, *9*, 1857.
- (80) Kumar, P. V.; Maroncelli, M. *J. Chem. Phys.* **1995**, *103*, 3038.
- (81) Ladanyi, B. M.; Maroncelli, M. *J. Chem. Phys.* **1998**, *109*, 3204.
- (82) The experimental correlation shown here excludes ionic liquids with the trihexyltetradecylphosphonium cation which shows anomalous behavior compared to the remaining liquids. For 15 ionic liquids (30 points) the correlation shown is $\langle \tau/\text{ps} \rangle = 1950\{\eta/T\}/(cP\cdot K^{-1})^{1.08}$.
- (83) Ito, N.; Arzhantsev, S.; Maroncelli, M. *Chem. Phys. Lett.* **2004**, *396*, 83.
- (84) Kashyap, H. K.; Biswas, R. *J. Phys. Chem. B* **2010**, *114*, 16811.
- (85) The simulation estimate of $C_\Delta(t)$ at 293 K was obtained using the temperature-dependent data on spherical solutes plotted in Figure 10b. Each of the $C_\Delta(t)$ functions was fit to eq 15 and the parameters f_G , ω_G , β , and $\ln(\tau_0/\text{ps})$ fit as linear or quadratic (τ_0) functions of temperature for both the charge (Δq) and the dipole ($\Delta\mu$) jump series. The average of the ratios $p_i(293 \text{ K})/p_i(350 \text{ K})$ of the Δq and $\Delta\mu$ data sets, where p_i represents the fitted value of parameter $p_i(T)$ was applied to the value of this parameter simulated for C153 at 350 K to obtain estimated values of the parameter at 293 K. The scaling factors for f_G , ω_G , β , and τ_0 so obtained were 0.98, 1.07, 12.3, and 0.96, respectively. Thus, the only appreciable change predicted was in τ_0 . The uncertainty in the τ_0 value so predicted is on the order of 50%.
- (86) Kashyap, H. K.; Biswas, R. *Indian J. Chem., Sect. A: Inorg., Bioinorg., Phys., Theor. Anal. Chem.* **2010**, *49A*, 685.
- (87) Maroncelli, M. *J. Chem. Phys.* **1991**, *94*, 2084.
- (88) Assuming linearity of the solvation energetics, the free energy or approximately the internal energy of the system is expected to decrease by $1/2\Delta U_{\text{El}}$ in all four perturbations. This energy will be initially deposited as the potential energy of solute–solvent and solvent–solvent interactions.
- (89) Given the fact that the cation dipole moment is only 3 D and that of the anion is zero, this modest influence of rotational motions is not unexpected in the present system or in most of the ionic liquids studied by these other authors. One would expect rotational dynamics to play a larger role for ionic liquids having higher dielectric constants and thus dipole moments than these model imidazolium liquids.
- (90) Schroeder, C.; Haberler, M.; Steinhauser, O. *J. Chem. Phys.* **2008**, *128*, 134501/1.
- (91) Decomposition of the response in reciprocal space provides a rigorous separation. Some discussion of such a decomposition for the neat ionic liquid is provided in ref 8.
- (92) Acree, W. E., Jr.; Abraham, M. H. *J. Chem. Technol. Biotechnol.* **2006**, *81*, 1441.
- (93) Schroeder, C.; Sonnleitner, T.; Buchner, R.; Steinhauser, O. *Phys. Chem. Chem. Phys.* **2011**, *13*, 12240.
- (94) See, however, the recent work by Sajadi et al.,⁹⁸ which suggests that solute motions could also play a role in determining solvation times in some conventional solvents.

(95) Jin, H.; O'Hare, B.; Dong, J.; Arzhantsev, S.; Baker, G. A.; Wishart, J. F.; Benesi, A. J.; Maroncelli, M. *J. Phys. Chem. B* **2010**, *115*, 1333.

(96) Marcus, Y. *The Properties of Solvents*; Wiley: New York, 1998.

(97) For example, the change in solvation energy caused by radial motion of a point charge $q = 0.78\text{ e}$ by 1 \AA is approximately 10 times larger than the change caused by a 30° rotation of a point dipole of 3.0 D .

(98) Sajadi, M.; Weinberger, M.; Wagenknecht, H.-A.; Ernsting, N. P. *Phys. Chem. Chem. Phys.* **2011**, *13*, 17768.